

# Hydrological variations of the intermediate water masses of the western Mediterranean Sea during the past 20 ka inferred from neodymium isotopic composition in foraminifera and cold-water corals

Quentin Dubois-Dauphin<sup>1</sup>, Paolo Montagna<sup>2,3</sup>, Giuseppe Siani<sup>1</sup>, Eric Douville<sup>4</sup>, Claudia Wienberg<sup>5</sup>, Dierk Hebbeln<sup>5</sup>, Zhifei Liu<sup>6</sup>, Nejib Kallel<sup>7</sup>, Arnaud Dapoigny<sup>4</sup>, Marie Revel<sup>8</sup>, Edwige Pons-Branchu<sup>4</sup>, Marco Taviani<sup>2,9</sup>, Christophe Colin<sup>1\*</sup>

<sup>1</sup>Laboratoire Geosciences Paris-Sud (GEOPS), Université de Paris Sud, Université Paris-Saclay, 91405 Orsay, France.

<sup>2</sup>ISMAR-CNR, via Gobetti 101, 40129 Bologna, Italy.

<sup>3</sup>Lamont-Doherty Earth Observatory, Columbia University, 61 Route 9W, Palisades, NY 10964, USA

<sup>4</sup>Laboratoire des Sciences du Climat et de l'Environnement, LSCE/IPSL, CEA-CNRS-UVSQ, Université Paris-Saclay, F-91191 Gif-sur-Yvette, France.

<sup>5</sup>MARUM-Center for Marine Environmental Sciences, University of Bremen, Leobener Strasse, 28359 Bremen, Germany.

<sup>6</sup>State Key Laboratory of Marine Geology, Tongji University, Shanghai 200092, China.

<sup>7</sup>Laboratoire Georessources, Matériaux, Environnements et Changements Globaux, LR13ES23, Faculté des Sciences de Sfax, Université de Sfax, BP1171, 3000 Sfax, Tunisia.

<sup>8</sup>Geoazur, UNS, IRD, OCA, CNRS, 250 rue Albert Einstein, 06500 Valbonne, France

<sup>9</sup>Biology Department, Woods Hole Oceanographic Institution, 266 Woods Hole Road, Woods Hole, MA 02543, USA.

Correspondence to: Christophe Colin ([christophe.colin@u-psud.fr](mailto:christophe.colin@u-psud.fr))

**Abstract.** We present the neodymium isotopic composition ( $\epsilon\text{Nd}$ ) of mixed planktonic foraminifera species from a sediment core collected at 622 m water depth in the Balearic Sea, as well as  $\epsilon\text{Nd}$  of scleractinian cold-water corals (CWC; *Madrepora oculata*, *Lophelia pertusa*) retrieved at 280–414 m water depth in the Alboran Sea and the south Sardinian continental margin. The aim is to constrain hydrological variations at intermediate depths in the western Mediterranean Sea during the last 20 kyr. Planktonic (*Globigerina bulloides*) and benthic (*Cibicidoides pachyderma*) foraminifera were also analyzed for stable oxygen ( $\delta^{18}\text{O}$ ) and carbon ( $\delta^{13}\text{C}$ ) isotopes. The foraminiferal and coral  $\epsilon\text{Nd}$  values from the Balearic and Alboran Sea are comparable over the last ~13 kyr, with mean values of  $-8.94 \pm 0.26$  ( $1\sigma$ ;  $n=24$ ) and  $-8.91 \pm 0.18$  ( $1\sigma$ ;  $n=25$ ), respectively. Before 13 ka BP, the foraminiferal  $\epsilon\text{Nd}$  values are slightly lower ( $-9.28 \pm 0.15$ ) and tend to reflect a higher mixing between intermediate and deep waters, which is characterized by more unradiogenic  $\epsilon\text{Nd}$  values. The slight  $\epsilon\text{Nd}$  increase after 13 ka BP is associated to a decoupling in the benthic foraminiferal  $\delta^{13}\text{C}$  composition between intermediate and deeper depths, which started at ~16 ka BP. This suggests an earlier stratification of the water masses and a subsequent reduced contribution of unradiogenic  $\epsilon\text{Nd}$  from deep waters. The CWC from the Sardinia Channel show a much larger scattering of  $\epsilon\text{Nd}$  values, from  $-8.66 \pm 0.30$  to  $-5.99 \pm 0.50$ , and a lower average ( $-7.31 \pm 0.73$ ;  $n=19$ ) compared to the CWC and foraminifera from the Alboran and Balearic Sea, indicative of intermediate waters sourced from the Levantine basin. At the time of sapropel S1 deposition (10.2 to 6.4 ka), the  $\epsilon\text{Nd}$  values of the Sardinian CWC become more unradiogenic ( $-8.38 \pm 0.47$ ;  $n=3$  at ~8.7 ka BP), suggesting a significant contribution of intermediate waters originated from the western basin. Accordingly, we propose that western

47 Mediterranean intermediate waters replaced the Levantine Intermediate Water (LIW), which was strongly  
48 reduced during the mid-sapropel (~8.7 ka BP). This observation supports a notable change of Mediterranean  
49 circulation pattern centered on sapropel S1 that needs further investigations to be confirmed.

50

## 51 **1. Introduction**

52 The Mediterranean Sea is a mid-latitude semi-enclosed basin, characterized by evaporation exceeding  
53 precipitation and river runoff, where the inflow of fresh and relatively warm surface Atlantic water is  
54 transformed into saltier and cooler (i.e. denser) intermediate and deep waters. Several studies have demonstrated  
55 that the Mediterranean thermohaline circulation was highly sensitive to both the rapid climatic changes  
56 propagated into the basin from high latitudes of the Northern Hemisphere (Cacho et al., 1999, 2000, 2002;  
57 Moreno et al., 2002, 2005; Paterne et al., 1999; Martrat et al., 2004; Sierro et al., 2005; Frigola et al., 2007,  
58 2008) and orbitally-forced modifications of the eastern Mediterranean freshwater budget mainly driven by  
59 monsoonal river runoff from the south (Rohling et al., 2002; 2004; Bahr et al., 2015). A link between the  
60 intensification of the Mediterranean Outflow Water (MOW) and the intensity of the Atlantic Meridional  
61 Overturning Circulation (AMOC) was proposed (Cacho et al., 1999, 2000, 2001; Bigg and Wadley, 2001; Sierro  
62 et al., 2005; Voelker et al., 2006) and recently supported by new geochemical data in sediments of the Gulf of  
63 Cádiz (Bahr et al., 2015). In particular, it has been suggested that the intensity of the MOW and, more generally,  
64 the variations of the thermohaline circulation of the Mediterranean Sea could play a significant role in triggering  
65 a switch from a weakened to an enhanced state of the AMOC through the injection of saline Mediterranean  
66 waters in the intermediate North Atlantic at times of weak AMOC (Rogerson et al., 2006; Voelker et al., 2006;  
67 Khélifi et al., 2009). The Mediterranean intermediate waters, notably the Levantine Intermediate Water (LIW),  
68 which represent today up to 80 % in volume of the MOW (Kinder and Parilla, 1987) are considered an important  
69 driver of MOW-derived salt into the North Atlantic. Furthermore, the LIW also plays a key role in controlling  
70 the deep-sea ventilation of the Mediterranean basin, being strongly involved in the formation of deep waters in  
71 the Aegean Sea, Adriatic Sea, Tyrrhenian Sea and Gulf of Lions (Millot and Taupier-Letage, 2005). It is  
72 hypothesized that a reduction of intermediate and deep-water formation as a consequence of surface hydrological  
73 changes in the eastern Mediterranean basin acted as a precondition for the sapropel S1 deposition by limiting the  
74 oxygen supply to the bottom waters (De Lange et al., 2008; Rohling et al., 2015; Tachikawa et al., 2015).  
75 Therefore, it is crucial to gain a more complete understanding of the variability of the Mediterranean  
76 intermediate circulation in the past and its impact on the MOW outflow and, in general, on the Mediterranean  
77 thermohaline circulation.

78 Previous studies have mainly focused on the glacial variability of the deep-water circulation in the western  
79 Mediterranean basin (Cacho et al., 2000, 2006; Sierro et al., 2005; Frigola et al., 2007, 2008). During the Last  
80 Glacial Maximum (LGM), strong deep-water convection took place in the Gulf of Lions, producing cold, well-  
81 ventilated western Mediterranean Deep Water (WMDW) (Cacho et al., 2000, 2006; Sierro et al., 2005), while  
82 the MOW flowed at greater depth in the Gulf of Cádiz (Rogerson et al., 2005; Schönfeld and Zahn, 2000). With  
83 the onset of the Termination 1 (T1) at about 15 ka, the WMDW production declined until the transition to the  
84 Holocene due to the rising sea level, with a relatively weak mode during the Heinrich Stadial 1 (HS1) and the  
85 Younger Dryas (YD) (Sierro et al., 2005; Frigola et al., 2008), that led to the deposition of the Organic Rich  
86 Layer 1 (ORL1; 14.5-8.2 ka BP; Cacho et al., 2002).

87 Because of the disappearance during the Early Holocene of specific epibenthic foraminiferal species, such as  
88 *Cibicoides* spp., which are commonly used for paleohydrological reconstructions, information about the  
89 Holocene variability of the deep-water circulation in the western Mediterranean are relatively scarce and are  
90 mainly based on grain size analysis and sediment geochemistry (e.g. Frigola et al., 2007). These authors have  
91 identified four distinct phases representing different deep-water overturning conditions in the western  
92 Mediterranean basin during the Holocene, as well as centennial- to millennial-scale abrupt events of overturning  
93 reinforcement.

94 Faunal and stable isotope records from benthic foraminifera located at intermediate depths in the eastern basin  
95 reveal uninterrupted well-ventilated LIW during the last glacial period and deglaciation (Kuhnt et al., 2008;  
96 Schmiedl et al., 2010). Similarly, a grain-size record obtained from a sediment core collected within the LIW  
97 depth range (~500 m water depth) at the east Corsica margin also documents enhanced bottom currents during  
98 the glacial period and for specific time intervals during the deglaciation, such as HS1 and YD (Toucanne et al.,  
99 2012). The Early Holocene is characterized by a collapse of the LIW (Kuhnt et al., 2008; Schmiedl et al., 2010;  
100 Toucanne et al., 2012) synchronous with the sapropel S1 deposition (10.2 – 6.4 cal ka BP; Mercone et al., 2000).  
101 Proxies for deep-water conditions reveal the occurrence of episodes of deep-water overturning reinforcement in  
102 the eastern Mediterranean basin at 8.2 ka BP (Rohling et al., 1997, 2015; Kuhnt et al., 2007; Abu-Zied et al.,  
103 2008, Siani et al., 2013; Tachikawa et al., 2015), responsible for the interruption of the sapropel S1 in the eastern  
104 Mediterranean basin (Mercone et al., 2001; Rohling et al., 2015).

105 Additional insights into Mediterranean circulation changes may be obtained using radiogenic isotopes, such as  
106 neodymium, that represent reliable tracers for constraining water-mass mixing and sources (Goldstein and  
107 Hemming, 2003, and references therein). It has recently been shown that the neodymium (Nd) isotopic  
108 composition, expressed as  $\epsilon\text{Nd} = \left( \frac{(^{143}\text{Nd}/^{144}\text{Nd})_{\text{sample}}}{(^{143}\text{Nd}/^{144}\text{Nd})_{\text{CHUR}}} - 1 \right) \times 10000$  (CHUR: Chondritic  
109 Uniform Reservoir [Jacobsen and Wasserburg, 1980]) of living and fossil scleractinian CWC faithfully traces  
110 intermediate and deep-water mass provenance and mixing of the ocean (e.g. van de Flierdt et al., 2010; Colin et  
111 al., 2010; López Correa et al., 2012; Monterro-Serrano et al., 2011, 2013; Copard et al., 2012). Differently from  
112 the CWC, the  $\epsilon\text{Nd}$  composition of fossil planktonic foraminifera is not related to the ambient seawater at  
113 calcification depths but reflects the bottom and/or pore water  $\epsilon\text{Nd}$ , due to the presence of authigenic Fe-Mn  
114 coatings precipitated on their carbonate shell (Roberts et al., 2010; Elmore et al., 2011; Piotrowski et al., 2012;  
115 Tachikawa et al., 2014; Wu et al., 2015). Therefore, the  $\epsilon\text{Nd}$  composition of planktonic foraminiferal tests can be  
116 used as a useful tracer of deep-water circulation changes in the past, although the effect of pore water on  
117 foraminiferal  $\epsilon\text{Nd}$  values could potentially complicate the interpretation (Tachikawa et al., 2014).

118 In the Mediterranean Sea, modern seawater  $\epsilon\text{Nd}$  values display a large range from ~-11 to ~-5, and a clear  
119 vertical and longitudinal gradient, with more radiogenic values encountered in the eastern basin and typically at  
120 intermediate and deeper depths (Spivack and Wasserburg 1988; Henry et al., 1994; Tachikawa et al., 2004;  
121 Vance et al., 2004). Considering this large  $\epsilon\text{Nd}$  contrast,  $\epsilon\text{Nd}$  recorded in fossil CWC and planktonic  
122 foraminifera from the Mediterranean offers great potential to trace intermediate and deep-water mass exchange  
123 between the two basins, especially during periods devoid of key epibenthic foraminifera, such as the sapropel S1  
124 or ORL1 events.

125 Here, the  $\epsilon\text{Nd}$  of planktonic foraminifera from a sediment core collected in the Balearic Sea and CWC samples  
126 from the Alboran Sea and the Sardinia Channel was investigated to establish past changes of the seawater  $\epsilon\text{Nd}$  at

127 intermediate depths and constrain hydrological variations of the LIW during the last ~20 kyr. The  $\epsilon\text{Nd}$  values  
128 have been combined with stable oxygen ( $\delta^{18}\text{O}$ ) and carbon ( $\delta^{13}\text{C}$ ) isotope measurements of benthic (*Cibicides*  
129 *pachyderma*) and planktonic (*Globigerina bulloides*) foraminifera and sea-surface temperature estimates by  
130 modern analogue technique (MAT). Results reveal significant  $\epsilon\text{Nd}$  variations at intermediate depths in the  
131 western basin interpreted as a drastic reduction of the hydrological exchanges between the western and eastern  
132 Mediterranean Sea and the subsequent higher proportion of intermediate water produced in the Gulf of Lions  
133 during the time interval corresponding to the sapropel S1 deposition.

134

135

## 136 2. Seawater $\epsilon\text{Nd}$ distribution in the Mediterranean Sea

137 The Atlantic Water (AW) enters the Mediterranean Sea as surface inflow through the Strait of Gibraltar with an  
138 unradiogenic  $\epsilon\text{Nd}$  signature of  $\sim -9.7$  in the strait (Tachikawa et al., 2004) and  $\sim -10.4$  in the Alboran Sea  
139 (Tachikawa et al., 2004, Spivack and Wasserburg, 1988) for depths shallower than 50 m. During its eastward  
140 flowing, AW mixes with upwelled Mediterranean Intermediate Water forming the Modified Atlantic Water  
141 (MAW) that spreads within the basin (Millot and Taupier-Letage, 2005) (Fig.1). The surface water  $\epsilon\text{Nd}$  values  
142 (shallower than 50 m) range from -9.8 to -8.8 in the western Mediterranean basin (Henry et al., 1994; Montagna  
143 et al., in prep) and -9.3 to -4.2 in the eastern basin, with seawater off the Nile delta showing the most radiogenic  
144 values (Tachikawa et al., 2004; Vance et al., 2004; Montagna et al., in prep). The surface waters in the eastern  
145 Mediterranean basin become denser due to strong mixing and evaporation caused by cold and dry air masses  
146 flowing over the Cyprus-Rhodes area in winter, and eventually sink leading to the formation of LIW  
147 (Ovchinnikov, 1984; Lascaratos et al., 1993, 1998; Malanotte-Rizzoli et al., 1999; Pinardi and Masetti, 2000).  
148 The LIW spreads throughout the entire Mediterranean basin at depths between  $\sim 150$ -200 m and  $\sim 600$ -700 m,  
149 and is characterized by more radiogenic  $\epsilon\text{Nd}$  values ranging from -7.9 to -4.8 (average value  $\pm 1\sigma$ :  $-6.6 \pm 1$ ) in  
150 the eastern basin and from -10.4 to -7.58 ( $-8.7 \pm 0.9$ ) in the western basin (Henry et al., 1994; Tachikawa et al.,  
151 2004; Vance et al., 2004; Montagna et al., in prep). The LIW acquires its  $\epsilon\text{Nd}$  signature mainly from the partial  
152 dissolution of Nile River particles (Tachikawa et al., 2004), which have an average isotopic composition of -3.25  
153 (Weldeab et al., 2002), and the mixing along its path with overlying and underlying water masses with different  
154  $\epsilon\text{Nd}$  signatures. The LIW finally enters the Atlantic Ocean at intermediate depths through the Strait of Gibraltar  
155 with an average  $\epsilon\text{Nd}$  value of  $-9.2 \pm 0.2$  (Tachikawa et al., 2004; Montagna et al., in prep).

156 The WMDW is formed in the Gulf of Lions due to winter cooling and evaporation followed by mixing between  
157 the relative fresh surface water and the saline LIW and spreads into the Balearic basin and Tyrrhenian Sea  
158 between  $\sim 2000$  m and 3000 m (Millot, 1999; Schroeder et al., 2013) (Fig. 1). The WMDW is characterized by an  
159 average  $\epsilon\text{Nd}$  value of  $-9.4 \pm 0.9$  (Henry et al., 1994; Tachikawa et al., 2004; Montagna et al., in prep). Between  
160 the WMDW and the LIW (from  $\sim 700$  to 2000 m), the Tyrrhenian Deep Water (TDW) has been found (Millot et  
161 al., 2006), which is produced by the mixing between WMDW and Eastern Mediterranean Deep Water (EMDW)  
162 that cascades in the Tyrrhenian Sea after entering from the Strait of Sicily (Millot, 1999, 2009; Astraldi et al.,  
163 2001). The TDW has an average  $\epsilon\text{Nd}$  value of  $-8.1 \pm 0.5$  (Montagna et al., in prep).

164

## 165 3. Material and methods

### 166 3.1. Cold-water coral and foraminifera samples

167 Forty-four CWC samples belonging to the species *Lophelia pertusa* and *Madrepora oculata* collected from the  
168 Alboran Sea and the Sardinia Channel were selected for this study (Fig. 1). Nineteen fragments were collected at  
169 various core depths from a coral-bearing sediment core (RECORD 23; 38°42.18' N; 08°54.75' E; Fig. 1)  
170 retrieved from 414 m water depth in the "Sardinian Cold-Water Coral Province" (Taviani et al., 2015) during the  
171 R/V Urania cruise "RECORD" in 2013. The core contains well-preserved fragments of *M. oculata* and *L.*  
172 *pertusa* embedded in a brownish muddy to silty carbonate-rich sediment. The Sardinian CWC samples were  
173 used for U-series dating and Nd isotopic composition measurements. For the southern Alboran Sea, twenty-five  
174 CWC samples were collected at water depths between 280 and 442 m in the "eastern Melilla Coral Province"  
175 (Fig. 1) during the R/V Poseidon cruise "POS-385" in 2009 (Hebbeln et al. 2009). Eleven samples were  
176 collected at the surface of two coral mounds (New Mound and Horse Mound) and three coral ridges (Brittlestar  
177 ridges I, II and III), using a box corer and a remotely operated vehicle (ROV). In addition, fourteen CWC  
178 samples were collected from various core depths of three coral-bearing sediment cores (GeoB13728, 13729 and  
179 13730) retrieved from the Brittlestar ridge I. Details on the location of surface samples and cores collected in the  
180 southern Alboran Sea and details on the radiocarbon ages obtained from these coral samples are reported in Fink  
181 et al. (2013). Like the CWC sample set from the Sardinia Channel, the dated Alboran CWC samples were also  
182 used for further Nd isotopic composition analyses in this study.

183 In addition, a deep-sea sediment core (barren of any CWC fragments) was recovered southwest of the Balearic  
184 Sea at 622 m water depth during the R/V Le Suroît cruise "PALEOCINAT II" in 1992 (SU92-33; 35°25.38' N;  
185 0°33.86' E; Fig. 1). The core unit, which consists of 2.1 m of grey to brown carbonaceous clays, was sub-  
186 sampled continuously at 5-10 cm intervals for a total number of 24 samples used for  $\delta^{18}\text{O}$ ,  $\delta^{13}\text{C}$  and  $\epsilon\text{Nd}$   
187 analyzes.

188

### 189 **3.2. Analytical procedures on cold-water coral samples**

#### 190 **3.2.1. U/Th dating**

191 The nineteen CWC samples collected from the sediment core RECORD 23 (Sardinia Channel) were analysed for  
192 uranium and thorium isotopes to obtain absolute dating using a Thermo Scientific<sup>TM</sup> Neptune<sup>Plus</sup> MC-ICPMS  
193 installed at the Laboratoire des Sciences du Climat et de l'Environnement (LSCE, Gif-sur-Yvette, France). Prior  
194 to analysis, the samples were carefully cleaned using a small diamond blade to remove any visible contamination  
195 and sediment-filled cavities. The fragments were examined under a binocular microscope to ensure against the  
196 presence of bioeroded zones and finally crushed into a coarse-grained powder with an agate mortar and pestle.  
197 The powders (~60-100 mg) were transferred to acid cleaned Teflon beakers, ultrasonicated in MilliQ water,  
198 leached with 0.1N HCl for ~ 15 s and finally rinsed twice with MilliQ water. The physically and chemically  
199 cleaned samples were dissolved in 3-4 ml dilute HCl (~10%) and mixed with an internal triple spike with known  
200 concentrations of  $^{229}\text{Th}$ ,  $^{233}\text{U}$  and  $^{236}\text{U}$ , calibrated against a Harwell Uraninite solution (HU-1) assumed to be at  
201 secular equilibrium. The solutions were evaporated to dryness at 70°C, redissolved in 0.6 ml 3N HNO<sub>3</sub> and then  
202 loaded into 500  $\mu\text{l}$  columns packed with Eichrom UTEVA resin to isolate uranium and thorium from the other  
203 major and trace elements of the carbonate matrix. The U and Th separation and purification followed a  
204 procedure slightly modified from Douville et al. (2010). The U and Th isotopes were determined following the  
205 protocol recently revisited at LSCE (Pons-Branchu et al., 2014). The  $^{230}\text{Th}/\text{U}$  ages were calculated from  
206 measured atomic ratios through iterative age estimation (Ludwig and Titterton, 1994), using the  $^{230}\text{Th}$ ,  $^{234}\text{U}$

207 and  $^{238}\text{U}$  decay constants of Cheng et al. (2013) and Jaffey et al. (1971). Due to the low  $^{232}\text{Th}$  concentration (< 1  
208 ng/g; see Table 1), no correction was applied for the non-radiogenic  $^{230}\text{Th}$  fraction.

209

### 210 3.2.2 Nd isotopic composition analyses on cold-water coral fragments

211 Sub-samples of the CWC fragments from the Sardinia Channel used for U-series dating in this study (Table 1) as  
212 well as sub-samples of the twenty-five CWC fragments originating from the Alboran Sea, which were already  
213 radiocarbon-dated by Fink et al. (2013) (Table 2), were used for further Nd isotopic composition analyses. The  
214 fragments (350 to 600 mg) were subjected to a mechanical and chemical cleaning procedure. The visible  
215 contaminations, such as Fe-Mn coatings and detrital particles, were carefully removed from the inner and  
216 outermost surfaces of the coral skeletons using a small diamond blade. The physically cleaned fragments were  
217 ultrasonicated for 10 min with 0.1 N ultra-clean HCl, followed by several MilliQ water rinses and finally  
218 dissolved in 2.5 N ultraclean  $\text{HNO}_3$ . Nd was separated from the carbonate matrix using Eichrom TRU and LN  
219 resins, following the analytical procedure described in detail in Copard et al. (2010).

220 The  $^{143}\text{Nd}/^{144}\text{Nd}$  ratios of all purified Nd fractions were analyzed using the ThermoScientific Neptune<sup>Plus</sup> Multi-  
221 Collector Inductively Coupled Plasma Mass Spectrometer (MC-ICP-MS) hosted at LSCE. The mass-  
222 fractionation correction was made by normalizing  $^{146}\text{Nd}/^{144}\text{Nd}$  to 0.7219 and applying an exponential law.  
223 During each analytical session, samples were systematically bracketed with analyses of JNdi-1 and La Jolla  
224 standard solutions, which are characterised by accepted values of  $0.512115 \pm 0.000006$  (Tanaka et al., 2000) and  
225  $0.511855 \pm 0.000007$  (Lugmair et al., 1983), respectively. Standard JNdi-1 and La Jolla solutions were analysed  
226 at concentrations similar to those of the samples (5-10 ppb) and all the measurements affected by instrumental  
227 bias were corrected, when necessary, using La Jolla standard. The external reproducibility ( $2\sigma$ ) for time resolved  
228 measurement, deduced from repeated analyses of La Jolla and JNdi-1 standards, ranged from 0.1 to 0.5  $\epsilon\text{Nd}$   
229 units for the different analytical sessions. The analytical error for each sample analysis was taken as the external  
230 reproducibility of the La Jolla standard for each session. Concentrations of Nd blanks were negligible compared  
231 to the amount of Nd of CWC investigated in this study.

232

## 233 3.3. Analyses on sediment of core SU92-33

### 234 3.3.1. Radiocarbon dating

235 Radiocarbon dating was measured at UMS-ARTEMIS (Pelletron 3MV) AMS (CNRS-CEA Saclay, France).  
236 Seven AMS radiocarbon ( $^{14}\text{C}$ ) dating were performed in core SU92-33 on well-preserved calcareous tests of the  
237 planktonic foraminifera *G. bulloides* in the size fraction >150  $\mu\text{m}$  (Table 3). The age model for the core was  
238 derived from the calibrated planktonic ages by applying a mean reservoir effect of ~400 years (Siani et al., 2000,  
239 2001). All  $^{14}\text{C}$  ages were converted to calendar years (cal. yr BP, BP = AD 1950) by using the INTCAL13  
240 calibration data set (Reimer et al., 2013) and the CALIB 7.0 program (Stuiver and Reimer, 1993).

241

### 242 3.3.2. Stable isotopes

243 Stable oxygen ( $\delta^{18}\text{O}$ ) and carbon ( $\delta^{13}\text{C}$ ) isotope measurements were performed in core SU92-33 on well-  
244 preserved (clean and intact) samples of the planktonic foraminifera *G. bulloides* (250-315  $\mu\text{m}$  fraction) and the  
245 epibenthic foraminifera *C. pachyderma* (250-315  $\mu\text{m}$  fraction) using a Finnigan MAT-253 mass spectrometer at  
246 the State Key Laboratory of Marine Geology (Tongji University). Both  $\delta^{18}\text{O}$  and  $\delta^{13}\text{C}$  values are presented

247 relative to the Pee Dee Belemnite (PDB) scale by comparison with the National Bureau of Standards (NBS) 18  
248 and 19. The mean external reproducibility was checked by replicate analyses of laboratory standards and is better  
249 than  $\pm 0.07\%$  ( $1\sigma$ ) for  $\delta^{18}\text{O}$  and  $\pm 0.04\%$  for  $\delta^{13}\text{C}$ .

### 250 3.3.3 *Nd isotope measurements on planktonic foraminifera*

251 Approximately 25 mg of mixed planktonic foraminifera species were picked from the  $>63\ \mu\text{m}$  size fraction of  
252 each sample already used for stable isotope measurements (Table 4). The samples were gently crushed between  
253 glass slides under the microscope to ensure that all chambers were open, and ultrasonicated with MilliQ water.  
254 Samples were allowed to settle between ultrasonication steps before removing the supernatant. Each sample was  
255 rinsed thoroughly with MilliQ water until the solution was clear and free of clay. The cleaned samples were  
256 dissolved in 1N acetic acid and finally centrifuged to ensure that all residual particles were removed, following  
257 the procedure described in Roberts et al. (2010). Nd was separated following the analytical procedure reported in  
258 Wu et al. (2015). For details on the measurement of Nd isotopes see the section above.

259

### 260 3.3.4. *Modern analogue technique (MAT)*

261 The palaeo-sea surface temperatures (SST) were estimated using the modern analogue technique (MAT)  
262 (Hutson, 1980; Prell, 1985), implemented by Kallel et al. (1997) for the Mediterranean Sea. This method directly  
263 measures the difference between the faunal composition of a fossil sample with a modern database, and it  
264 identifies the best modern analogues for each fossil assemblage (Prell, 1985). Reliability of SST reconstructions  
265 is estimated using a square chord distance test (dissimilarity coefficient), which represents the mean degree of  
266 similarity between the sample and the best 10 modern analogues. When the dissimilarity coefficient is lower than  
267 0.25, the reconstruction is considered to be of good quality (Overpeck et al., 1985; Kallel et al., 1997). For core  
268 SU92-33, good dissimilarity coefficients are  $<0.2$ , with an average value of  $\sim 0.13$  (varying between 0.07 and  
269 0.19; Fig. 2a). The calculated mean standard deviation of SST estimates observed in core MD90-917 are  $\sim 1.5$   
270  $^{\circ}\text{C}$  from the late glacial period to the Younger Dryas and  $\sim 1.2\ ^{\circ}\text{C}$  for the Holocene.

271

## 272 4. Results

### 273 4.1. *Cold-water corals*

274 The good state of preservation for the CWC samples from the Sardinia Channel (RECORD 23; Fig. 1) is attested  
275 by their initial  $\delta^{234}\text{U}$  values (Table 1), which is in the range of the modern seawater value ( $146.8\pm 0.1$ ; Andersen  
276 et al., 2010). If the uncertainty of the  $\delta^{234}\text{U}_i$  is taken into account, all the values fulfill the so-called “strict”  $\pm 4$   
277  $\%$  reliability criterion and the U/Th ages can be considered strictly reliable. The coral ages range from  
278  $0.091\pm 0.011$  to  $10.904\pm 0.042$  ka BP (Table 1), and reveal three distinct clusters of coral age distribution during  
279 the Holocene representing periods of sustained coral occurrence. These periods coincide with the Early Holocene  
280 encompassing a 700-years-lasting time interval from  $\sim 10.9$  to  $10.2$  ka BP, the very late Early Holocene at  $\sim 8.7$   
281 ka BP, and the Late Holocene starting at  $\sim 1.5$  ka BP (Table 1).

282 Radiocarbon ages obtained for CWC samples collected in the Alboran Sea were published by Fink et al. (2013)  
283 (Table 2). They also document three periods of sustained CWC occurrence coinciding with the Bølling–Allerød  
284 (B-A) interstadial (13.5–12.9 cal ka BP), the Early Holocene (11.2–9.8 cal ka BP) and the Mid- to Late Holocene  
285 (5.4–0.3 cal ka BP).

286 The  $\epsilon\text{Nd}$  record obtained from the CWC samples from the Alboran Sea displays a narrow range from  $-9.22\pm 0.30$   
287 to  $-8.59\pm 0.3$ , which is comparable to the  $\epsilon\text{Nd}$  record of the planktonic foraminifera from the Balearic Sea over  
288 the last 13.5 kyr (Table 2, Fig. 3b). Most of the CWC  $\epsilon\text{Nd}$  values are similar within error and the record does not  
289 reveal any clear difference over the last  $\sim 13.5$  kyr.

290 On the contrary, the CWC samples from the Sardinia Channel display a relatively large  $\epsilon\text{Nd}$  range, with values  
291 varying from  $-5.99\pm 0.50$  to  $-7.75\pm 0.10$  during the Early and Late Holocene, and values as low as  $-8.66\pm 0.30$   
292 during the the mid-sapropel S1 deposition (S1a) at  $\sim 8.7$  ka BP (Table 1, Fig. 3c).

293

294

#### 295 **4.2 Core SU92-33**

296 The stratigraphy of core SU92-33 was derived from the  $\delta^{18}\text{O}$  variations of the planktonic foraminifera  
297 *G. bulloides* (Fig. 2b). The last glacial/interglacial transition and the Holocene encompasses the upper 2.1 m of  
298 the core (Fig. 2b). The  $\delta^{18}\text{O}$  record of *G. bulloides* shows higher values ( $\sim 3.5$  ‰) during the late glacial  
299 compared to the Holocene (from  $\sim 1.5$  to  $0.8$  ‰) exhibiting a pattern similar to those observed in nearby deep-sea  
300 cores from the Western Mediterranean Sea (Sierro et al., 2005; Melki et al., 2009).

301 The age model for the upper 1.2 m of the core SU92-33 was based on 7 AMS- $^{14}\text{C}$  age measurements and a  
302 linear interpolation between these ages (Table 3, Fig. 2). For the lower portion of the core, a control point was  
303 established at the onset of the last deglaciation, which is coeval in the western and central Mediterranean Sea at  
304  $\sim 17$  cal ka BP (Sierro et al., 2005; Melki et al., 2009; Siani et al., 2001). Overall, the upper 2.1 m of core SU92-  
305 33 spans the last 19 kyr, with an estimated average sedimentation rate ranging from  $\sim 15$  cm  $\text{ka}^{-1}$  during the  
306 deglaciation to  $\sim 10$  cm  $\text{ka}^{-1}$  during the Holocene.

307 April-May SST reconstruction was derived from MAT to define the main climatic events recorded in  
308 core SU92-33 during the last 19 kyr. SST vary from  $8.5^\circ\text{C}$  to  $17.5^\circ\text{C}$  with high amplitude variability over the last  
309 19 kyr BP (Fig. 2a). The LGM (19-18 ka BP) is characterized by SST values centered at around  $12^\circ\text{C}$ . Then, a  
310 progressive decrease of  $\sim 4^\circ\text{C}$  between 17.8 ka and 16 ka marks the Heinrich Stadial 1 (HS1) (Fig. 2a). A  
311 warming phase ( $\sim 14^\circ\text{C}$ ) between 14.5 ka BP and 13.8 ka BP coincides with the B-A interstadial and is followed  
312 by a cooling ( $\sim 11^\circ\text{C}$ ) between 13.1 ka BP and 11.8 ka BP largely corresponding to the YD (Fig. 2a). During the  
313 Holocene, SST show mainly values of  $\sim 16^\circ\text{C}$ , with one exception between 7 ka BP and 6 ka BP pointing to an  
314 abrupt cooling of  $\sim 3^\circ\text{C}$  (Fig. 2a). From the late glacial to the Holocene, SST variations show a similar pattern to  
315 that previously observed in the Gulf of Lions and Tyrrhenian Sea (Kallel et al., 1997; Melki et al., 2009) as well  
316 as in the Alboran Sea (Martrat et al., 2014; Rodrigo-Gámiz et al., 2014). They are globally synchronous for the  
317 main climatic transitions to the well dated South Adriatic Sea core MD90-917 (Siani et al., 2004) confirming the  
318 robustness of the SU92-33 age model (Fig. 2a).

319 The  $\delta^{18}\text{O}$  and  $\delta^{13}\text{C}$  records obtained from the benthic foraminifera *C. pachyderma* display significant variations  
320 at millennial time scales (Figs. 2c and 2d). The  $\delta^{18}\text{O}$  values decrease steadily from  $\sim 4.5$  ‰ during the LGM to  
321  $\sim 1.5$  ‰ during the Holocene, without showing any significant excursion during HS1 and the YD events (Fig.  
322 2c), in agreement with results obtained from the neighbor core MD99-2343 (Sierro et al., 2005).

323 The  $\delta^{13}\text{C}$  record of *C. pachyderma* shows a decreasing trend since the LGM with a low variability from  $\sim 1.6$  ‰  
324 to  $\sim 0.6$  ‰ (Fig. 2d). The heaviest  $\delta^{13}\text{C}$  values are related to the LGM ( $\sim 1.6$  ‰) while the lightest values ( $\sim 0.6$



325 ‰) characterize the Early Holocene and in particular the period corresponding to the sapropel S1 event in the  
326 eastern Mediterranean basin (Fig. 2d).

327 The  $\epsilon\text{Nd}$  values of planktonic foraminifera of core SU92-33 from the Balearic Sea vary within a relatively  
328 narrow range between  $-9.50\pm 0.30$  and  $-8.61\pm 0.30$ , with an average value of  $-9.06\pm 0.28$  (Table 2, Fig. 3b). The  
329 record shows a slight increasing trend since the LGM, with the more unradiogenic values (average  $-9.28\pm 0.15$ ;  
330  $n=7$ ) being observed in the oldest part of the record (between 18 and 13.5 ka BP), whereas Holocene values are  
331 generally more radiogenic (average  $-8.84\pm 0.22$ ;  $n=17$ ) (Fig. 3b).

332

### 333 **5. Discussion**

334 Overall, the CWC and foraminiferal  $\epsilon\text{Nd}$  values measured in this study point to a pronounced dispersion at  
335 intermediate depth in terms of absolute values and variability in Nd isotopes during the Holocene between the  
336 Alboran and Balearic Seas and the Sardinia Channel. Furthermore, the foraminiferal  $\epsilon\text{Nd}$  record reveals an  
337 evolution towards more radiogenic values at intermediate water depth in the Balearic Sea over the last ~19 kyr  
338 (Fig. 3).

339 A prerequisite to properly interpret such  $\epsilon\text{Nd}$  differences and variations through time consists in characterizing  
340 first the present-day  $\epsilon\text{Nd}$  of the main water-mass end-members flowing in the western Mediterranean basin. It is  
341 also necessary to evaluate the temporal changes in  $\epsilon\text{Nd}$  of the end-members since the LGM, and assess the  
342 potential influences of lithogenic Nd input and regional exchange between the continental margins and seawater  
343 (“boundary exchange”; Lacan and Jeandel, 2001, 2005) on the  $\epsilon\text{Nd}$  values of intermediate water masses.

344 During its westward flow, the LIW continuously mixes with surrounding waters with different  $\epsilon\text{Nd}$  signatures  
345 lying above and below. For the western Mediterranean basin, these water masses are the MAW/Western  
346 Intermediate Water (WIW) and the TDW/WMDW, respectively. Accordingly, a well-defined and gradual  $\epsilon\text{Nd}$   
347 gradient exists at intermediate depth between the eastern and western Mediterranean basins, with LIW values  
348 becoming progressively more unradiogenic towards the Strait of Gibraltar, from  $-4.8\pm 0.2$  at 227 m in the  
349 Levantine basin to  $-10.4\pm 0.2$  at 200 m in the Alboran Sea (Tachikawa et al., 2004). Such an  $\epsilon\text{Nd}$  pattern implies  
350 an effective vertical mixing with more unradiogenic water masses along the E-W LIW trajectory ruling out  
351 severe isotopic modifications of the LIW due to the local exchange between the continental margins and  
352 seawater. Unfortunately, no information exists on the potential temporal variability in  $\epsilon\text{Nd}$  of the Mediterranean  
353 water-mass end-members since the LGM.

354 It has been demonstrated that eolian dust input can modify the surface and sub-surface  $\epsilon\text{Nd}$  distribution of the  
355 ocean in some areas (Arsouze et al., 2009). The last glacial period was associated with an aridification of North  
356 Africa (Sarnthein et al., 1981; Hooghiemstra et al., 1987; Moreno et al., 2002; Wienberg et al., 2010) and higher  
357 fluxes of Saharan dust to the NE tropical Atlantic (Itambi et al., 2009) and the western Mediterranean Sea  
358 characterized by unradiogenic  $\epsilon\text{Nd}$  values (between  $-11\pm 0.4$  and  $-14\pm 0.4$ ; see synthesis in Scheuvens et al.,  
359 2013). Bout-Roumazeilles et al. (2013) documented a dominant role of eolian supply in the Siculo-Tunisian  
360 Strait during the last 20 ka, with the exception of a significant riverine contribution (from the Nile River) and a  
361 strong reduction of eolian input during the sapropel S1 event. Such variations in the eolian input to the  
362 Mediterranean Sea are not associated to a significant change in the seawater  $\epsilon\text{Nd}$  record obtained for the Balearic  
363 Sea (core SU92-33) during the sapropel S1 event (Fig. 3). Furthermore, the  $\epsilon\text{Nd}$  signature of the CWC from the  
364 Sardinia Channel (core RECORD 23) shifts to more unradiogenic values ( $-8.66\pm 0.30$ ) during the sapropel S1

365 event, which is opposite to what expected if it was related to a strong reduction of eolian sediment input. In a  
366 recent study, Rodrigo-Gámiz et al. (2015) have documented variations in the terrigenous provenance from a  
367 sediment record in the Alboran Sea (core 293G; 36°10.414'N, 2°45.280'W, 1840 m water depth) since the  
368 LGM. Radiogenic isotopes (Sr, Nd, Pb) point to changes from North African dominated sources during the  
369 glacial period to European dominated source during the Holocene. Nevertheless, the major Sr-Nd-Pb excursions  
370 documented by Rodrigo-Gámiz et al. (2015) and dated at ca. 11.5, 10.2, 8.9-8.7, 5.6, 2.2 and 1.1. ka cal BP do  
371 not seem to affect the  $\epsilon\text{Nd}$  values of our foraminifera and coral records.

372 Taken together, these results suggest that changes of eolian dust input since the LGM were not responsible for  
373 the observed  $\epsilon\text{Nd}$  variability at intermediate water depths.

374 Consequently, assuming that the Nd isotopic budget of the western Mediterranean Sea has not been strongly  
375 modified since the LGM, the reconstructed variations of the E-W gradient of  $\epsilon\text{Nd}$  values in the western  
376 Mediterranean Sea for the past and notably during the sapropel S1 event (Fig. 3) are indicative of a major  
377 reorganization of intermediate water circulation.

378

### 379 ***5.1 Hydrological changes in the Alboran and Balearic Seas since the LGM***

380 The range in  $\epsilon\text{Nd}$  for the CWC from the Alboran Sea (from  $-9.22\pm 0.30$  to  $-8.8.59\pm 0.30$ ; Table 2) is very close to  
381 the one obtained for the planktonic foraminifera from the Balearic Sea (from  $-9.50\pm 0.30$  to  $-8.61\pm 0.30$ ; Table 4,  
382 Fig. 3c), suggesting that both sites are influenced by the same intermediate water masses at least for the last 13.5  
383 kyr BP. Today, LIW occupies a depth range between  $\sim 200$  and  $\sim 700$  m in the western Mediterranean basin  
384 (Millot, 1999; Sparnocchia et al., 1999). More specifically, the salinity maximum corresponding to the core of  
385 LIW is found at around 400 m in the Alboran Sea (Millot, 2009) and up to 550 m in the Balearic Sea (López-  
386 Jurado et al., 2008). The youngest CWC sample collected in the Alboran Sea with a rather "recent" age of 0.34  
387 cal ka BP (Fink et al. 2013) displays an  $\epsilon\text{Nd}$  value of  $-8.59\pm 0.30$  (Table 2) that is similar to the present-day value  
388 of the LIW at the same site ( $-8.3\pm 0.2$ ) (Dubois-Dauphin et al., submitted) and is significantly different from the  
389 WMDW  $\epsilon\text{Nd}$  signature in the Alboran Sea ( $-10.7\pm 0.2$ , 1270 m water depth; Tachikawa et al., 2004). Considering  
390 the intermediate depth range of the studied CWC and foraminifera samples, we can reasonably assume that  
391 samples from both sites, in the Balearic Sea (622 m water depth) and in the Alboran Sea (280 to 442 m water  
392 depth), record  $\epsilon\text{Nd}$  variations of the LIW. The  $\epsilon\text{Nd}$  record obtained from planktonic foraminifera generally  
393 displays more unradiogenic and homogenous values before  $\sim 13$  cal ka BP (range from  $-9.46$  to  $-9.12$ ) compared  
394 to the most recent part of the record (range from  $-9.50$  to  $-8.61$ ), with the highest value of  $-8.61\pm 0.3$  in the Early  
395 and Late Holocene.

396 The SST record displays values centered at around  $12^\circ\text{C}$  during the LGM with a subsequent rapid SST decrease  
397 towards  $9^\circ\text{C}$ , highlighting the onset of the HS1 (Fig. 2a). These values are well comparable to recent high-  
398 resolution SST data obtained in the Alboran Sea (Martrat et al., 2014; Rodrigo-Gámiz et al., 2014).

399 The  $\delta^{18}\text{O}$  record obtained on *G. bulloides* indicates an abrupt 1‰ excursion towards lighter values centered at  
400 about 16 cal ka BP (Table 4), synchronous with the HS1 (Fig. 2b), which is similar to the  $\delta^{18}\text{O}$  shift reported by  
401 Sierró et al. (2005) for a core collected at 2391 m water depth NE of the Balearic Islands (MD99-2343; Fig. 1).  
402 As the Heinrich events over the last glacial period are characterized by colder and fresher surface water in the  
403 Alboran Sea (Cacho et al., 1999; Pérez-Folgado et al., 2003; Martrat et al., 2004, 2014; Rodrigo-Gámiz et al.,  
404 2014) and dry climate on land over the western Mediterranean Sea (Allen et al., 1999; Combourieu-Nebout et

405 al., 2002; Sanchez Goni et al., 2002; Bartov et al., 2003), lighter  $\delta^{18}\text{O}$  values of planktonic *G. bulloides* are  
406 thought to be the result of the inflow of freshwater derived from the melting of icebergs in the Atlantic Ocean  
407 into the Mediterranean Sea (Sierro et al., 2005; Rogerson et al., 2008).

408 During this time interval, the  $\delta^{13}\text{C}$  record of *C. pachyderma* from the Balearic Sea (core SU92-33) displays a  
409 decreasing  $\delta^{13}\text{C}$  trend after ~16 cal ka BP (from 1.4 ‰ to 0.9 ‰; Table 4; Fig. 4a). Moreover, the  $\delta^{13}\text{C}$  record  
410 obtained on benthic foraminifera *C. pachyderma* from the deep Balearic Sea (core MD99-2343) reveals similar  
411  $\delta^{13}\text{C}$  values before ~16 cal ka BP suggesting well-mixed and ventilated water masses during the LGM and the  
412 onset of the deglaciation (Sierro et al., 2005).

413 The slightly lower foraminiferal  $\epsilon\text{Nd}$  values before ~13 cal ka BP could reflect a stronger influence of water  
414 masses deriving from the Gulf of Lions as WMDW ( $\epsilon\text{Nd}$ :  $-9.4\pm 0.9$ ; Henry et al., 1994; Tachikawa et al., 2004;  
415 Montagna et al., in prep). This is in agreement with  $\epsilon\text{Nd}$  results obtained by Jiménez-Espejo et al. (2015) from  
416 planktonic foraminifera collected from deep-water sites (1989 m and 2382 m) in the Alboran Sea (Fig. 4c).  
417 Jiménez-Espejo et al. (2015) documented lower  $\epsilon\text{Nd}$  values (ranging from  $-10.14\pm 0.27$  to  $-9.58\pm 0.22$ ) during the  
418 LGM, suggesting an intense deep-water formation. This is also associated to an enhanced activity of the deeper  
419 branch of the MOW in the Gulf of Cádiz (Rogerson et al., 2005; Voelker et al., 2006) linked to the active  
420 production of the WMDW in the Gulf of Lions during the LGM (Jiménez-Espejo et al., 2015).

421 The end of the HS1 (14.7 cal ka BP) is concurrent with the onset of the B-A warm interval characterized by  
422 increased SST up to 14°C in the Balearic Sea (SU92-33; Fig. 3a), also identified for various sites in the  
423 Mediterranean Sea (Cacho et al., 1999; Martrat et al., 2004, 2014; Essallami et al., 2007; Rodrigo-Gámiz et al.,  
424 2014). The B-A interval is associated with the so-called melt-water pulse 1A (e.g. Weaver et al., 2003) occurring  
425 at around 14.5 cal ka BP. This led to a rapid sea-level rise of about 20 m in less than 500 years and large  
426 freshwater discharges in the Atlantic Ocean due to the melting of continental ice sheets (Deschamps et al., 2012),  
427 resulting in an enhanced Atlantic inflow across the Strait of Gibraltar. Synchronously, cosmogenic dating of  
428 Alpine glacier retreat throughout the western Mediterranean hinterland suggests maximum retreat rates (Ivy-  
429 Ochs et al., 2007; Kelly et al., 2006). Overall, these events are responsible for freshening Mediterranean waters  
430 and reduced surface water density, and hence, weakened ventilation of intermediate (Toucanne et al., 2012) and  
431 deep-water masses (Cacho et al., 2000; Sierro et al., 2005). Similarly, lower benthic  $\delta^{13}\text{C}$  values obtained for the  
432 Balearic Sea (Fig. 4a) point to less ventilated intermediate water relative to the late glacial. In addition, a  
433 decoupling in the benthic  $\delta^{13}\text{C}$  values is observed between deep (MD99-2343) and intermediate (core SU92-33)  
434 waters after ~16 cal ka BP (Sierro et al. 2005), suggesting an enhanced stratification of the waters masses (Fig.  
435 4a). At this time, the shallowest  $\epsilon\text{Nd}$  record from the deep Alboran Sea (core 300G) shifted towards more  
436 radiogenic values, while the deepest one (core 304G) remained close to the LGM values (Jimenez-Espejo et al.,  
437 2015) (Fig. 4c). Furthermore, results from the UP10 fraction (particles > 10  $\mu\text{m}$ ) of the MD99-2343 sediment  
438 core (Fig. 4d) indicate a declining bottom-current velocity at 15 ka BP (Frigola et al., 2008). Rogerson et al.  
439 (2008) have hypothesized that during deglacial periods the sinking depth of dense waters produced in the Gulf of  
440 Lions was shallower resulting in new intermediate water (WIW) rather than new deep-water (WMDW) as  
441 observed today during mild winters (Millot, 1999; Schott et al., 1996). Therefore, intermediate depths of the  
442 Balearic Sea could have been isolated from the deep-water with the onset of the T1 (at ~15 ka BP). The reduced  
443 convection in the deep western Mediterranean Sea together with the shoaling of the nutricline (Rogerson et al.,  
444 2008) led to the deposition of the ORL 1 (14.5 to 8.2 ka B.P; Cacho et al., 2002) and dysoxic conditions below

445 2000 m in agreement with the absence of epibenthic foraminifera such as *C. pachyderma* after 11 cal ka BP in  
446 MD99-2343 (Sierro et al., 2005) (Fig. 4a).

447 After 13.5 ka BP, planktonic foraminifera  $\epsilon\text{Nd}$  values from the Balearic Sea (core SU92-33) become more  
448 radiogenic and are in the range of CWC  $\epsilon\text{Nd}$  values from the Alboran Sea (Fig. 4b). These values may reveal a  
449 stronger influence of the LIW in the Balearic Sea during the Younger Dryas, as also supported by the sortable  
450 silt record from the Tyrrhenian Sea (Toucanne et al., 2012) (Fig. 4e). Deeper depths of the Alboran Sea also  
451 record a stronger influence of the LIW with an  $\epsilon\text{Nd}$  value of  $-9.1\pm 0.4$  (Jimenez-Espejo et al., 2015). In addition,  
452 a concomitant activation of the upper MOW branch, as reconstructed from higher values of Zr/Al ratio in  
453 sediments of the Gulf of Cádiz, can be related to the enhanced LIW flow in the western Mediterranean Sea (Fig.  
454 4f) (Bahr et al., 2015).

455 The time of sapropel S1 deposition (10.2 – 6.4 ka) is characterized by a weakening or a shutdown of  
456 intermediate- and deep-water formation in the eastern Mediterranean basin (Rossignol-Strick et al., 1982; Cramp  
457 and O’Sullivan, 1999; Emeis et al., 2000; Rohling et al., 2015). At this time, planktonic foraminifera  $\epsilon\text{Nd}$  values  
458 from intermediate water depths in the Balearic Sea (core SU92-33) remain high (between  $-9.15\pm 0.3$  and  
459  $-8.61\pm 0.3$ ) (Fig. 4b). On the other hand, the deeper Alboran Sea provides a value of  $-9.8\pm 0.3$  pointing to a  
460 stronger contribution of WMDW (Jimenez-Espejo et al., 2015), coeval with the recovery of deep-water activity  
461 from core MD99-2343 (Frigola et al., 2008).

462

### 463 **5.2 Hydrological changes in the Sardinia Channel during the Holocene**

464 The present-day hydrographic structure of the Sardinia Channel is characterized by four water masses, with the  
465 surface, intermediate and deep-water masses being represented by MAW, LIW and TDW/WMDW, respectively  
466 (Astraldi et al., 2002a; Millot and Taupier-Lepage, 2005). In addition, the WIW, flowing between the MAW and  
467 the LIW, has also been observed along the Channel (Sammari et al., 1999). The core of the LIW is located at  
468 400-450 m water depth in the Tyrrhenian Sea (Hopkins, 1988; Astraldi et al., 2002b), which is the depth range of  
469 CWC samples from the Sardinia Channel (RECORD 23; 414 m) (Taviani et al., 2015). The youngest CWC  
470 sample dated at  $\sim 0.1$  ka BP has an  $\epsilon\text{Nd}$  value of  $-7.70\pm 0.10$  (Table 1, Fig. 5), which is similar within error to the  
471 value obtained from a seawater sample collected at 451 m close to the coral sampling location ( $-8.0\pm 0.4$ ;  
472 Montagna et al., in prep).

473 The CWC dating from the Sardinia Channel shows three distinct periods of sustained coral occurrence in this  
474 area during the Holocene, with each displaying a large variability in  $\epsilon\text{Nd}$  values. CWC from the Early Holocene  
475 (10.9-10.2 ka BP) and the Late Holocene ( $<1.5$  ka BP) exhibit similar ranges of  $\epsilon\text{Nd}$  values (ranging from  
476  $-5.99\pm 0.50$  to  $-7.75\pm 0.20$ ; Table 1, Fig 5c). Such variations are within the present-day  $\epsilon\text{Nd}$  range being  
477 characteristic for intermediate waters in the eastern Mediterranean Sea ( $-6.6\pm 1.0$ ; Tachikawa et al., 2004; Vance  
478 et al., 2004). However, the CWC  $\epsilon\text{Nd}$  values are more radiogenic than those observed at mid-depth in the  
479 present-day western basin (ranging from  $-10.4\pm 0.2$  to  $-7.58\pm 0.47$ ; Henry et al., 1994; Tachikawa et al., 2004;  
480 Montagna et al., in prep), suggesting a stronger LIW component in the Sardinia Channel during the Early and  
481 Late Holocene. The Sardinian CWC  $\epsilon\text{Nd}$  variability also reflects the sensitivity of the LIW to changes in the  
482 eastern basin such as rapid variability of the Nile River flood discharge (Revel et al., 2014; 2015; Weldeab et al.,  
483 2014) or a modification through time in the proportion between the LIW and the Cretan Intermediate Water  
484 (CIW). Today, the intermediate water outflowing from the Strait of Sicily is composed by  $\sim 66$  to 75 % of LIW

485 and 33 to 25 % of CIW (Manca et al., 2006; Millot, 2014). As the CIW is formed in the Aegean Sea, this  
486 intermediate water mass is generally more radiogenic than LIW (Tachikawa et al., 2004; Montagna et al., in  
487 prep). Following this hypothesis, a modification of the mixing proportion between the CIW and the LIW may  
488 potentially explain values as radiogenic as about -6 in the Sardinia Channel during the Early and Late Holocene  
489 (Fig. 5c). However, a stronger LIW and/or a CIW contribution cannot be responsible for  $\epsilon\text{Nd}$  values as low as -  
490  $8.66 \pm 0.30$  observed during the sapropel S1 event at 8.7 ka BP (Table 1, Fig. 5c). Considering that such  
491 unradiogenic value is not observed at intermediate depth in the modern eastern Mediterranean basin, the most  
492 plausible hypothesis suggested here is that the CWC were influenced by a higher contribution of intermediate  
493 water from the western basin.

494

### 495 *5.3 Hydrological implications for the intermediate water masses of the western Mediterranean Sea*

496 The  $\epsilon\text{Nd}$  records of the Balearic Sea, Alboran Sea and Sardinia Channel document a temporal variability of the  
497 east-west gradient in the western Mediterranean basin during the Holocene. The magnitude of the gradient  
498 ranges from  $\sim 1.5$  to  $\sim 3$   $\epsilon$  units during the Early and Late Holocene and it is strongly reduced at 8.7 ka BP,  
499 coinciding with the sapropel S1 event affecting the eastern Mediterranean basin (Fig. 5). Such variations could  
500 be the result of a modification of the Nd isotopic composition of intermediate water masses due to changes of the  
501 LIW production through time and a higher contribution of the western-sourced intermediate water towards the  
502 Sardinia Channel coinciding with the sapropel S1 event.

503 The LIW acquires its radiogenic  $\epsilon\text{Nd}$  in the Mediterranean Levantine basin mainly from Nd exchange between  
504 seawater and lithogenic particles originating mainly from Nile River (Tachikawa et al., 2004). A higher sediment  
505 supply from the Nile River starting at  $\sim 15$  ka BP was documented by a shift to more radiogenic  $\epsilon\text{Nd}$  values of  
506 the terrigenous fraction obtained from a sediment core having been influenced by the Nile River discharge  
507 (Revel et al., 2015) (Fig. 5e). Others studies pointed to a gradual enhanced Nile River runoff as soon as 14.8 ka  
508 BP and a peak of Nile discharge from 9.7 to 8.4 ka recorded by large increase in sedimentation rate from 9.7 to  
509 8.4 ka ( $>120$  cm/ka) (Revel et al., 2015; Weldeab et al., 2014; Castaneda et al., 2016). Similarly, enhanced Nile  
510 discharge at  $\sim 9.5$  cal kyr B.P was inferred based on  $\delta^{18}\text{O}$  in planktonic foraminifera from a sediment core in the  
511 southeast Levantine Basin (PS009PC ( $32^\circ 07.7'N$ ,  $34^\circ 24.4'E$ ; 552 m water depth) (Hennekam et al., 2014). This  
512 increasing contribution of the Nile River to the eastern Mediterranean basin has been related to the African  
513 Humid Period (14.8–5.5 ka BP; Shanahan et al., 2015), which in turn was linked to the precessional increase in  
514 Northern Hemisphere insolation during low eccentricity (deMenocal et al., 2000; Barker et al., 2004; Garcin et  
515 al., 2009). An increasing amount of radiogenic sediments dominated by the Blue/Atbara Nile River contribution  
516 (Revel et al., 2014) could have modified the  $\epsilon\text{Nd}$  of surface water towards more radiogenic values (Revel et al.,  
517 in prep). Indeed, planktonic foraminifera  $\epsilon\text{Nd}$  values as high as  $\sim -3$  have been documented in the eastern  
518 Levantine Basin (ODP site 967;  $34^\circ 04.27'N$ ,  $32^\circ 43.53'E$ ; 2553 m water depth) during the sapropel S1 event as a  
519 result of enhanced Nile flooding (Scrivner et al., 2004). The radiogenic signature was likely transferred to  
520 intermediate depth as a consequence of the LIW formation in the Rhodes Gyre, and it might have been  
521 propagated westwards towards the Sardinia Channel.

522 Therefore, considering the more unradiogenic value of the CWC samples from the Sardinia Channel during the  
523 sapropel S1a event, it is very unlikely that eastern-sourced water flowed at intermediate depth towards the  
524 Sardinia Channel. A possible explanation could be the replacement of the radiogenic LIW that was no longer

525 produced in the eastern basin (Rohling, 1994) by less radiogenic western intermediate water (possibly WIW).  
526 Such a scenario could even support previous hypotheses that invoke a potential circulation reversal in the eastern  
527 Mediterranean from anti-estuarine to estuarine during sapropel formation (Huang and Stanley, 1972; Calvert,  
528 1983; Sarmiento et al., 1988; Buckley and Johnson, 1988; Thunell and Williams, 1989). An alternative  
529 hypothesis would be that reduced surface water densities in the eastern Mediterranean during sapropel S1  
530 resulted in the LIW sinking to shallower depths than at present. As a result of this shoaling, CWC from the  
531 Sardinia Channel would have been bathed by underlying Western Intermediate Water during the sapropel S1a  
532 event.

533

## 534 **6. Conclusions**

535 The foraminiferal  $\epsilon\text{Nd}$  record from intermediate depths in the Balearic Sea reveals a relatively narrow range of  
536  $\epsilon\text{Nd}$  values varying between -9.50 and -8.61 since the LGM (~20 ka). Between 18 and 13.5 cal ka BP, the more  
537 unradiogenic  $\epsilon\text{Nd}$  values support a vigorous deep overturning in the Gulf of Lions while  $\delta^{18}\text{O}$  and  $\delta^{13}\text{C}$  values  
538 indicate a stratification of the water masses after 16 cal ka BP. The stratification together with a decrease of the  
539 deep-water intensity led to more radiogenic values after ~13 cal ka BP. The foraminiferal  $\epsilon\text{Nd}$  record, supported  
540 by  $\epsilon\text{Nd}$  values from CWC in the Alboran Sea, shows only minor changes in neodymium isotopes from 13.5 cal  
541 ka BP to 0.34 cal ka BP, suggesting that the westernmost part of the western Mediterranean basin is not very  
542 sensitive to hydrological variations of the LIW.

543 On the contrary, CWC located at the depth of the LIW in the Sardinia Channel exhibit large  $\epsilon\text{Nd}$  variations  
544 (between  $-7.75\pm 0.10$  and  $-5.99\pm 0.50$ ) during the Holocene, suggesting either the role of the Nile River in  
545 changing the  $\epsilon\text{Nd}$  of the LIW in the eastern Mediterranean basin or a variable LIW/CIW mixing of the water  
546 outflowing from the Strait of Sicily. At the time of the sapropel S1 event at ~8.7 ka BP, CWC display a shift  
547 toward lower values ( $-8.66\pm 0.30$ ), similar to those obtained at intermediate depths in the westernmost part of the  
548 western basin. This suggests that western-sourced intermediate water likely filled mid-depth of the southern  
549 Sardinia, replacing LIW that was no longer produced (or heavily reduced) in the eastern basin. These results  
550 could potentially support a reversal of the Mediterranean circulation, although this assumption needs further  
551 investigation to be confirmed.

552

## 553 **Acknowledgements**

554 The research leading to this study has received funding from the French National Research Agency  
555 “Investissement d’Avenir” (n°ANR-10-LABX-0018), the HAMOC project ANR-13-BS06-0003, the  
556 MISTRALS/PALEOMEX/COFIMED and ENVIMED/Boron Isotope and Trace Elements project. This work  
557 contributes to the RITMARE project. We thank Hiske Fink for selecting and kindly providing the cold-water  
558 corals samples from the Alboran Sea. We further thank François Thil and Louise Bordier for their support with  
559 Nd isotopic composition analyses. Paolo Montagna is grateful for financial support from the Short Term  
560 Mobility Program (CNR). Thanks are also extended to the captains, crews, chief scientists, and scientific parties  
561 of research cruises RECORD (R/V Urania), POS-385 (R/V Poseidon) and PALEOCINAT II (R/V Le Suroît).

562

563 **References**

- 564 Abu-Zied, R. H., Rohling, E. J., Jorissen, F. J., Fontanier, C., Casford, J. S. L. and Cooke, S.: Benthic  
565 foraminiferal response to changes in bottom-water oxygenation and organic carbon flux in the eastern  
566 Mediterranean during LGM to Recent times, *Mar. Micropaleontol.*, 67(1-2), 46–68,  
567 doi:10.1016/j.marmicro.2007.08.006, 2008.
- 568 Allen, J. R. M., Huntley, B., Brandt, U., Brauer, A., Hubberten, H., Keller, J., Kraml, M., Mackensen, A.,  
569 Mingram, J., Negendank, J. F. W., Nowaczyk, N. R., Oberhänsli, H., Watts, W. A., Wulf, S. and Zolitschka, B.:  
570 Rapid environmental changes in southern Europe during the last glacial period, *Nature*, 400(6746), 740–743,  
571 doi:10.1038/23432, 1999.
- 572 Andersen, M. B., Stirling, C. H., Zimmermann, B. and Halliday, A. N.: Precise determination of the open ocean  
573 <sup>234</sup>U/<sup>238</sup>U composition, *Geochemistry, Geophys. Geosystems*, 11(12), Q12003, doi:10.1029/2010GC003318,  
574 2010.
- 575 Arsouze, T., Dutay, J.-C., Lacan, F. and Jeandel, C.: Reconstructing the Nd oceanic cycle using a coupled  
576 dynamical – biogeochemical model, *Biogeosciences*, 6(12), 2829–2846, doi:10.5194/bg-6-2829-2009, 2009.
- 577 Astraldi, M., Gasparini, G. P., Gervasio, L. and Salusti, E.: Dense Water Dynamics along the Strait of Sicily  
578 (Mediterranean Sea), *J. Phys. Oceanogr.*, 31(12), 3457–3475, doi:10.1175/1520-  
579 0485(2001)031<3457:DWDATS>2.0.CO;2, 2001.
- 580 Astraldi, M., Gasparini, G. P., Vetrano, A. and Vignudelli, S.: Hydrographic characteristics and interannual  
581 variability of water masses in the central Mediterranean: A sensitivity test for long-term changes in the  
582 Mediterranean Sea, *Deep. Res. Part I Oceanogr. Res. Pap.*, 49(4), 661–680, doi:10.1016/S0967-0637(01)00059-  
583 0, 2002a.
- 584 Astraldi, M., Conversano, F., Civitarese, G., Gasparini, G. P., Ribera d’Alcalà, M. and Vetrano, a.: Water mass  
585 properties and chemical signatures in the central Mediterranean region, *J. Mar. Syst.*, 33-34, 155–177,  
586 doi:10.1016/S0924-7963(02)00057-X, 2002b.
- 587 Bahr, A., Kaboth, S., Jiménez-Espejo, F. J., Sierro, F. J., Voelker, A. H. L., Lourens, L., Röhl, U., Reichert, G.  
588 J., Escutia, C., Hernández-Molina, F. J., Pross, J. and Friedrich, O.: Persistent monsoonal forcing of  
589 Mediterranean Outflow Water dynamics during the late Pleistocene, *Geology*, 43(11), 951–954,  
590 doi:10.1130/G37013.1, 2015.
- 591 Barker, P. A., Talbot, M. R., Street-Perrott, F. A., Marret, F., Scourse, J. and Odada, E. O.: Late Quaternary  
592 climatic variability in intertropical Africa, in *Past Climate Variability through Europe and Africa*, pp. 117–138,  
593 Springer Netherlands, Dordrecht., 2004.
- 594 Bartov, Y., Goldstein, S. L., Stein, M. and Enzel, Y.: Catastrophic arid episodes in the Eastern Mediterranean  
595 linked with the North Atlantic Heinrich events, *Geology*, 31(5), 439, doi:10.1130/0091-  
596 7613(2003)031<0439:CAEITE>2.0.CO;2, 2003.

597 Bigg, G. R. and Wadley, M. R.: Millennial-scale variability in the oceans: an ocean modelling view, *J. Quat.*  
598 *Sci.*, 16(4), 309–319, doi:10.1002/jqs.599, 2001.

599 Bout-Roumazeilles, V., Combourieu-Nebout, N., Desprat, S., Siani, G., Turon, J. L. and Essallami, L.: Tracking  
600 atmospheric and riverine terrigenous supplies variability during the last glacial and the Holocene in central  
601 Mediterranean, *Clim. Past*, 9(3), 1065–1087, doi:10.5194/cp-9-1065-2013, 2013.

602 Buckley, H. A. and Johnson, L. R.: Late pleistocene to recent sediment deposition in the central and western  
603 Mediterranean, *Deep Sea Res. Part A. Oceanogr. Res. Pap.*, 35(5), 749–766, doi:10.1016/0198-0149(88)90028-  
604 3, 1988.

605 Cacho, I., Pelejero, C., Grimalt, J. O., Calafat, A. and Canals, M.: C37 alkenone measurements of sea surface  
606 temperature in the Gulf of Lions (NW Mediterranean), *Org. Geochem.*, 30(7), 557–566, doi:10.1016/S0146-  
607 6380(99)00038-8, 1999.

608 Cacho, I., Grimalt, J. O., Sierro, F. J., Shackleton, N. and Canals, M.: Evidence for enhanced Mediterranean  
609 thermohaline circulation during rapid climatic coolings, *Earth Planet. Sci. Lett.*, 183(3-4), 417–429,  
610 doi:10.1016/S0012-821X(00)00296-X, 2000.

611 Cacho, I., Grimalt, J. O., Canals, M., Sbaiffi, L., Shackleton, N. J., Schönfeld, J. and Zahn, R.: Variability of the  
612 western Mediterranean Sea surface temperature during the last 25,000 years and its connection with the Northern  
613 Hemisphere climatic changes, *Paleoceanography*, 16(1), 40–52, doi:10.1029/2000PA000502, 2001.

614 Cacho, I., Grimalt, J. O. and Canals, M.: Response of the Western Mediterranean Sea to rapid climatic variability  
615 during the last 50,000 years: a molecular biomarker approach, *J. Mar. Syst.*, 33-34, 253–272,  
616 doi:10.1016/S0924-7963(02)00061-1, 2002.

617 Cacho, I., Shackleton, N., Elderfield, H., Sierro, F. J. and Grimalt, J. O.: Glacial rapid variability in deep-water  
618 temperature and  $\delta^{18}\text{O}$  from the Western Mediterranean Sea, *Quat. Sci. Rev.*, 25(23-24), 3294–3311,  
619 doi:10.1016/j.quascirev.2006.10.004, 2006.

620 Calvert, S. E.: Geochemistry of Pleistocene sapropels and associated sediments from the Eastern Mediterranean,  
621 *Oceanol. Acta*, 6(3), 255–267, 1983.

622 Castañeda, I. S., Schouten, S., Pätzold, J., Lucassen, F., Kasemann, S., Kuhlmann, H. and Schefuß, E.:  
623 Hydroclimate variability in the Nile River Basin during the past 28,000 years, *Earth Planet. Sci. Lett.*, 438, 47–  
624 56, doi:10.1016/j.epsl.2015.12.014, 2016.

625 Cheng, H., Lawrence Edwards, R., Shen, C.-C., Polyak, V. J., Asmerom, Y., Woodhead, J. D., Hellstrom, J.,  
626 Wang, Y., Kong, X., Spötl, C., Wang, X. and Calvin Alexander, E.: Improvements in  $^{230}\text{Th}$  dating,  $^{230}\text{Th}$  and  
627  $^{234}\text{U}$  half-life values, and U–Th isotopic measurements by multi-collector inductively coupled plasma mass  
628 spectrometry, *Earth Planet. Sci. Lett.*, 371-372, 82–91, doi:10.1016/j.epsl.2013.04.006, 2013.

629 Colin, C., Frank, N., Copard, K. and Douville, E.: Neodymium isotopic composition of deep-sea corals from the  
630 NE Atlantic: implications for past hydrological changes during the Holocene, *Quat. Sci. Rev.*, 29(19-20), 2509–



631 2517, doi:10.1016/j.quascirev.2010.05.012, 2010.

632 Combourieu-Nebout, N., Turon, J. L., Zahn, R., Capotondi, L., Londeix, L. and Pahnke, K.: Enhanced aridity  
633 and atmospheric high-pressure stability over the western Mediterranean during the North Atlantic cold events of  
634 the past 50 k.y, *Geology*, 30(10), 863–866, doi:10.1130/0091-7613(2002)030<0863:EAAAHP>2.0.CO;2, 2002.

635 Copard, K., Colin, C., Douville, E., Freiwald, A., Gudmundsson, G., De Mol, B. and Frank, N.: Nd isotopes in  
636 deep-sea corals in the North-eastern Atlantic, *Quat. Sci. Rev.*, 29(19-20), 2499–2508,  
637 doi:10.1016/j.quascirev.2010.05.025, 2010.

638 Copard, K., Colin, C., Henderson, G. M., Scholten, J., Douville, E., Sicre, M.-A. and Frank, N.: Late Holocene  
639 intermediate water variability in the northeastern Atlantic as recorded by deep-sea corals, *Earth Planet. Sci. Lett.*,  
640 313-314, 34–44, doi:10.1016/j.epsl.2011.09.047, 2012.

641 Cramp, A. and O’Sullivan, G.: Neogene sapropels in the Mediterranean: a review, *Mar. Geol.*, 153(1-4), 11–28,  
642 doi:10.1016/S0025-3227(98)00092-9, 1999.

643 De Lange, G. J., Thomson, J., Reitz, A., Slomp, C. P., Principato, M. S., Erba, E. and Corselli, C.: Synchronous  
644 basin-wide formation and redox-controlled preservation of a Mediterranean sapropel, *Nat. Geosci.*, 1(9), 606–  
645 610, 2008.

646 DeMenocal, P., Ortiz, J., Guilderson, T. and Sarnthein, M.: Coherent High- and Low-Latitude Climate  
647 Variability During the Holocene Warm Period, *Science* (80-. ), 288(5474), 2198–2202,  
648 doi:10.1126/science.288.5474.2198, 2000.

649 Deschamps, P., Durand, N., Bard, E., Hamelin, B., Camoin, G., Thomas, A. L., Henderson, G. M., Okuno, J. and  
650 Yokoyama, Y.: Ice-sheet collapse and sea-level rise at the Bølling warming 14,600 years ago, *Nature*,  
651 483(7391), 559–564, doi:10.1038/nature10902, 2012.

652 Douville, E., Sallé, E., Frank, N., Eisele, M., Pons-Branchu, E. and Ayrault, S.: Rapid and accurate U–Th dating  
653 of ancient carbonates using inductively coupled plasma-quadrupole mass spectrometry, *Chem. Geol.*, 272(1-4),  
654 1–11, doi:10.1016/j.chemgeo.2010.01.007, 2010.

655 Dubois-Dauphin, Q., Colin, C., Bonneau, L., Montagna, P., Wu, Q., Van Rooij, D., Reverdin, G., Douville, E.,  
656 Thil, F., Waldner, A., Frank, N.: Fingerprinting North-east Atlantic water masses using Neodymium isotopes,  
657 *EPSL*, Submitted.

658

659 Elmore, A. C., Piotrowski, A. M., Wright, J. D. and Scrivner, A. E.: Testing the extraction of past seawater Nd  
660 isotopic composition from North Atlantic deep sea sediments and foraminifera, *Geochemistry, Geophys.*  
661 *Geosystems*, 12(9), doi:10.1029/2011GC003741, 2011.

662 Emeis, K.-C., Sakamoto, T., Wehausen, R. and Brumsack, H.-J.: The sapropel record of the eastern  
663 Mediterranean Sea — results of Ocean Drilling Program Leg 160, *Palaeogeogr. Palaeoclimatol. Palaeoecol.*,  
664 158(3-4), 371–395, doi:10.1016/S0031-0182(00)00059-6, 2000.

665 Fink, H. G., Wienberg, C., De Pol-Holz, R., Wintersteller, P. and Hebbeln, D.: Cold-water coral growth in the  
666 Alboran Sea related to high productivity during the Late Pleistocene and Holocene, *Mar. Geol.*, 339, 71–82,  
667 doi:10.1016/j.margeo.2013.04.009, 2013.

668 Frigola, J., Moreno, A., Cacho, I., Canals, M., Sierro, F. J., Flores, J. a., Grimalt, J. O., Hodell, D. a. and Curtis,  
669 J. H.: Holocene climate variability in the western Mediterranean region from a deepwater sediment record,  
670 *Paleoceanography*, 22(2), n/a–n/a, doi:10.1029/2006PA001307, 2007.

671 Frigola, J., Moreno, A., Cacho, I., Canals, M., Sierro, F. J., Flores, J. A. and Grimalt, J. O.: Evidence of abrupt  
672 changes in Western Mediterranean Deep Water circulation during the last 50kyr: A high-resolution marine  
673 record from the Balearic Sea, *Quat. Int.*, 181(1), 88–104, doi:10.1016/j.quaint.2007.06.016, 2008.

674 Garcin, Y., Junginger, A., Melnick, D., Olago, D. O., Strecker, M. R. and Trauth, M. H.: Late Pleistocene–  
675 Holocene rise and collapse of Lake Suguta, northern Kenya Rift, *Quat. Sci. Rev.*, 28(9-10), 911–925,  
676 doi:10.1016/j.quascirev.2008.12.006, 2009.

677 Hebbeln, D., Wienberg, C., Beuck, L., Freiwald, A., Wintersteller, P. and cruise participants (2009) Report and  
678 preliminary results of R/V POSEIDON Cruise 385 "Cold-water corals of the Alboran Sea (western  
679 Mediterranean Sea)", *Faro - Toulon*, 29.5. - 16.6.2009. Reports of the Department of Geosciences at the  
680 University of Bremen, No. 273. Department of Geosciences, Bremen University. urn:nbn:de:gbv:46-  
681 ep000106508.

682 Hennekam, R., Jilbert, T., Schnetger, B. and De Lange, G. J.: Solar forcing of Nile discharge and sapropel S1  
683 formation in the early to middle Holocene eastern Mediterranean, *Paleoceanography*, 29(5), 343–356,  
684 doi:10.1002/2013PA002553, 2014.

685 Henry, F., Jeandel, C., Dupré, B. and Minster, J.-F.: Particulate and dissolved Nd in the western Mediterranean  
686 Sea: Sources, fate and budget, *Mar. Chem.*, 45(4), 283–305, doi:10.1016/0304-4203(94)90075-2, 1994.

687 Hooghiemstra, H., Bechler, A. and Beug, H.-J.: Isopollen maps for 18,000 years B.P. of the Atlantic offshore of  
688 northwest Africa: Evidence for paleowind circulation, *Paleoceanography*, 2, 561–582,  
689 doi:10.1029/PA002i006p00561, 1987.

690 Hopkins, T. S.: Recent observations on the intermediate and deep water circulation in the Southern Tyrrhenian  
691 Sea, *Oceanol. Acta*, (Special issue), 41–50, 1988.

692 Huang, T. C. and Stanley, D. J.: Western Alboran sea: sediment dispersal, pouncing and reversal of currents, in  
693 *The Mediterranean Sea: A Natural Sedimentation Laboratory*, pp. 521–559, Dowden, Hutchinson & Ross,  
694 Stroudsburg, PA., 1972.

695 Hutson, W. H.: The Agulhas Current During the Late Pleistocene: Analysis of Modern Faunal Analogs, *Science*  
696 (80-. ), 207(4426), 64–66, doi:10.1126/science.207.4426.64, 1980.

697 Itambi, a. C., von Dobeneck, T., Mulitza, S., Bickert, T. and Heslop, D.: Millennial-scale northwest African  
698 droughts related to Heinrich events and Dansgaard-Oeschger cycles: Evidence in marine sediments from

699 offshore Senegal, *Paleoceanography*, 24(1), PA1205, doi:10.1029/2007PA001570, 2009.

700 Ivy-Ochs, S., Kerschner, H. and Schlüchter, C.: Cosmogenic nuclides and the dating of Lateglacial and Early  
701 Holocene glacier variations: The Alpine perspective, *Quat. Int.*, 164-165, 53–63,  
702 doi:10.1016/j.quaint.2006.12.008, 2007.

703 Jacobsen, S. B. and Wasserburg, G. J.: Sm-Nd isotopic evolution of chondrites, *Earth Planet. Sci. Lett.*, 50(1),  
704 139–155, doi:10.1016/0012-821X(80)90125-9, 1980.

705 Jaffey, A. H., Flynn, K. F., Glendenin, L. E., Bentley, W. C. and Essling, A. M.: Precision measurements of half-  
706 lives and specific activities of <sup>235</sup>U and <sup>238</sup>U, *Phys. Rev. C*, 4(5), 1889–1906, doi:10.1103/PhysRevC.4.1889,  
707 1971.

708 Jiménez-Espejo, F. J., Pardos-Gené, M., Martínez-Ruiz, F., García-Alix, A., van de Flierdt, T., Toyofuku, T.,  
709 Bahr, A. and Kreissig, K.: Geochemical evidence for intermediate water circulation in the westernmost  
710 Mediterranean over the last 20kyrBP and its impact on the Mediterranean Outflow, *Glob. Planet. Change*, 135,  
711 38–46, doi:10.1016/j.gloplacha.2015.10.001, 2015.

712 Kallel, N., Paterne, M., Labeyrie, L., Duplessy, J.-C. and Arnold, M.: Temperature and salinity records of the  
713 Tyrrhenian Sea during the last 18,000 years, *Palaeogeogr. Palaeoclimatol. Palaeoecol.*, 135(1-4), 97–108,  
714 doi:10.1016/S0031-0182(97)00021-7, 1997.

715 Kelly, M. A., Ivy-Ochs, S., Kubik, P. W., Von Blanckenburg, F. and Schlüchter, C.: Chronology of deglaciation  
716 based on 10 Be dates of glacial erosional features in the Grimsel Pass region, central Swiss Alps, *Boreas*, 35(4),  
717 634–643, doi:10.1111/j.1502-3885.2006.tb01169.x, 2006.

718 Khelifi, N., Sarnthein, M., Andersen, N., Blanz, T., Frank, M., Garbe-Schonberg, D., Haley, B. a., Stumpf, R.  
719 and Weinelt, M.: A major and long-term Pliocene intensification of the Mediterranean outflow, 3.5-3.3 Ma ago,  
720 *Geology*, 37(9), 811–814, doi:10.1130/G30058A.1, 2009.

721 Kinder, T. H. and Parrilla, G.: Yes, some of the Mediterranean water does come from great depth, *J. Geophys.*  
722 *Res.*, 92, 2901–2906, doi:10.1029/JC092iC03p02901, 1987.

723 Kuhnt, T., Schmiedl, G., Ehrmann, W., Hamann, Y. and Hemleben, C.: Deep-sea ecosystem variability of the  
724 Aegean Sea during the past 22 kyr as revealed by Benthic Foraminifera, *Mar. Micropaleontol.*, 64(3-4), 141–  
725 162, doi:10.1016/j.marmicro.2007.04.003, 2007.

726 Kuhnt, T., Schmiedl, G., Ehrmann, W., Hamann, Y. and Andersen, N.: Stable isotopic composition of Holocene  
727 benthic foraminifers from the Eastern Mediterranean Sea: Past changes in productivity and deep water  
728 oxygenation, *Palaeogeogr. Palaeoclimatol. Palaeoecol.*, 268(1-2), 106–115, doi:10.1016/j.palaeo.2008.07.010,  
729 2008.

730 Lacan, F. and Jeandel, C.: Tracing Papua New Guinea imprint on the central Equatorial Pacific Ocean using  
731 neodymium isotopic compositions and Rare Earth Element patterns, *Earth Planet. Sci. Lett.*, 186(3-4), 497–512,  
732 doi:10.1016/S0012-821X(01)00263-1, 2001.

- 733 Lacan, F. and Jeandel, C.: Neodymium isotopes as a new tool for quantifying exchange fluxes at the continent–  
734 ocean interface, *Earth Planet. Sci. Lett.*, 232(3-4), 245–257, doi:10.1016/j.epsl.2005.01.004, 2005.
- 735 Lascaratos, A. and Nittis, K.: A high-resolution three-dimensional numerical study of intermediate water  
736 formation in the Levantine Sea, *J. Geophys. Res.*, 103(C9), 18497, doi:10.1029/98JC01196, 1998.
- 737 Lascaratos, A., Williams, R. G. and Tragou, E.: A mixed-layer study of the formation of Levantine intermediate  
738 water, *J. Geophys. Res.*, 98(C8), 14739, doi:10.1029/93JC00912, 1993.
- 739 López Correa, M., Montagna, P., Joseph, N., Rüggeberg, A., Fietzke, J., Flögel, S., Dorschel, B., Goldstein, S.  
740 L., Wheeler, A. and Freiwald, A.: Preboreal onset of cold-water coral growth beyond the Arctic Circle revealed  
741 by coupled radiocarbon and U-series dating and neodymium isotopes, *Quat. Sci. Rev.*, 34, 24–43,  
742 doi:10.1016/j.quascirev.2011.12.005, 2012.
- 743 López-Jurado, J. L., Marcos, M. and Monserrat, S.: Hydrographic conditions affecting two fishing grounds of  
744 Mallorca island (Western Mediterranean): during the IDEA Project (2003-2004), *J. Mar. Syst.*, 71(3-4), 303–  
745 315, doi:10.1016/j.jmarsys.2007.03.007, 2008.
- 746 Ludwig, K. R. and Titterton, D. M.: Calculation of <sup>230</sup>Th/U isochrons, ages, and errors, *Geochim.*  
747 *Cosmochim. Acta*, 58(22), 5031–5042, doi:http://dx.doi.org/10.1016/0016-7037(94)90229-1, 1994.
- 748 Lugmair, G. W., Shimamura, T., Lewis, R. S. and Anders, E.: Samarium-146 in the Early Solar System:  
749 Evidence from Neodymium in the Allende Meteorite, *Science (80-. )*, 222(4627), 1015–1018,  
750 doi:10.1126/science.222.4627.1015, 1983.
- 751 Malanotte-Rizzoli, P., Manca, B. B., D’Alcala, M. R., Theocharis, A., Brenner, S., Budillon, G. and Ozsoy, E.:  
752 The Eastern Mediterranean in the 80s and in the 90s: the big transition in the intermediate and deep circulations,  
753 *Dyn. Atmos. Ocean.*, 29(2-4), 365–395, doi:10.1016/S0377-0265(99)00011-1, 1999.
- 754 Manca, B., Ibello, V., Pacciaroni, M., Scarazzato, P. and Giorgetti, A.: Ventilation of deep waters in the Adriatic  
755 and Ionian Seas following changes in thermohaline circulation of the Eastern Mediterranean, *Clim. Res.*, 31,  
756 239–256, doi:10.3354/cr031239, 2006.
- 757 Martrat, B., Grimalt, J. O., Lopez-Martinez, C., Cacho, I., Sierro, F. J., Flores, J. A., Zahn, R., Canals, M.,  
758 Curtis, J. H. and Hodell, D. a: Abrupt temperature changes in the Western Mediterranean over the past 250,000  
759 years., *Science (80-. )*, 306(5702), 1762–1765, doi:10.1126/science.1101706, 2004.
- 760 Martrat, B., Jimenez-Amat, P., Zahn, R. and Grimalt, J. O.: Similarities and dissimilarities between the last two  
761 deglaciations and interglaciations in the North Atlantic region, *Quat. Sci. Rev.*, 99, 122–134,  
762 doi:10.1016/j.quascirev.2014.06.016, 2014.
- 763 Melki, T., Kallel, N., Jorissen, F. J., Guichard, F., Dennielou, B., Berné, S., Labeyrie, L. and Fontugne, M.:  
764 Abrupt climate change, sea surface salinity and paleoproductivity in the western Mediterranean Sea (Gulf of  
765 Lion) during the last 28 kyr, *Palaeogeogr. Palaeoclimatol. Palaeoecol.*, 279(1-2), 96–113,  
766 doi:10.1016/j.palaeo.2009.05.005, 2009.

- 767
- 768 Mercone, D., Thomson, J., Croudace, I. W., Siani, G., Paterne, M. and Troelstra, S.: Duration of S1, the most  
769 recent sapropel in the eastern Mediterranean Sea, as indicated by accelerator mass spectrometry radiocarbon and  
770 geochemical evidence, *Paleoceanography*, 15(3), 336–347, doi:10.1029/1999PA000397, 2000.
- 771 Mercone, D., Thomson, J., Abu-Zied, R. H., Croudace, I. W. and Rohling, E. J.: High-resolution geochemical  
772 and micropalaeontological profiling of the most recent eastern Mediterranean sapropel, *Mar. Geol.*, 177(1-2),  
773 25–44, doi:10.1016/S0025-3227(01)00122-0, 2001.
- 774 Millot, C.: Circulation in the Western Mediterranean Sea, *J. Mar. Syst.*, 20(1-4), 423–442, doi:10.1016/S0924-  
775 7963(98)00078-5, 1999.
- 776 Millot, C.: Another description of the Mediterranean Sea outflow, *Prog. Oceanogr.*, 82(2), 101–124,  
777 doi:10.1016/j.pocean.2009.04.016, 2009.
- 778 Millot, C.: Heterogeneities of in- and out-flows in the Mediterranean Sea, *Prog. Oceanogr.*, 120, 254–278,  
779 doi:10.1016/j.pocean.2013.09.007, 2014.
- 780 Millot, C. and Taupier-Letage, I.: Circulation in the Mediterranean Sea, in *Environmental Chemistry*, vol. 5,  
781 edited by A. Saliot, pp. 29–66, Springer Berlin Heidelberg, Heidelberg., 2005.
- 782 Millot, C., Candela, J., Fuda, J.-L. and Tber, Y.: Large warming and salinification of the Mediterranean outflow  
783 due to changes in its composition, *Deep Sea Res. Part I Oceanogr. Res. Pap.*, 53(4), 656–666,  
784 doi:10.1016/j.dsr.2005.12.017, 2006.
- 785 Montero-Serrano, J.-C., Frank, N., Colin, C., Wienberg, C. and Eisele, M.: The climate influence on the mid-  
786 depth Northeast Atlantic gyres viewed by cold-water corals, *Geophys. Res. Lett.*, 38(19),  
787 doi:10.1029/2011GL048733, 2011.
- 788 Montero-Serrano, J.-C., Frank, N., Tisnérat-Laborde, N., Colin, C., Wu, C., Lin, K., Shen, C., Copard, K.,  
789 Orejas, C., Gori, A., De Mol, L., Van Rooij, D., Reverdin, G. and Douville, E.: Decadal changes in the mid-  
790 depth water mass dynamic of the Northeastern Atlantic margin (Bay of Biscay), *Earth Planet. Sci. Lett.*, 364,  
791 134–144, doi:10.1016/j.epsl.2013.01.012, 2013.
- 792 Moreno, A., Cacho, I., Canals, M., Prins, M. a., Sánchez-Goñi, M.-F., Grimal, O. J. and Weltje, G. J.: Saharan  
793 Dust Transport and High-Latitude Glacial Climatic Variability: The Alboran Sea Record, *Quat. Res.*, 58, 318–  
794 328, doi:10.1006/qres.2002.2383, 2002.
- 795 Moreno, A., Cacho, I., Canals, M., Grimalt, J. O., Sánchez-Goñi, M. F., Shackleton, N. and Sierro, F. J.: Links  
796 between marine and atmospheric processes oscillating on a millennial time-scale. A multi-proxy study of the last  
797 50,000yr from the Alboran Sea (Western Mediterranean Sea), *Quat. Sci. Rev.*, 24(14-15), 1623–1636,  
798 doi:10.1016/j.quascirev.2004.06.018, 2005.
- 799 Myers, P. G., Haines, K. and Rohling, E. J.: Modeling the paleocirculation of the Mediterranean: The Last  
800 Glacial Maximum and the Holocene with emphasis on the formation of sapropel S1, *Paleoceanography*, 13(6),

801 586–606, doi:10.1029/98PA02736, 1998.

802 Ovchinnikov, I. M.: The formation of intermediate water in the Mediterranean, *Oceanology*, 24, 168–173, 1984.

803 Overpeck, J. T., Webb, T. and Prentice, I. C.: Quantitative interpretation of fossil pollen spectra: Dissimilarity  
804 coefficients and the method of modern analogs, *Quat. Res.*, 23(1), 87–108, doi:10.1016/0033-5894(85)90074-2,  
805 1985.

806 Paterne, M., Kallel, N., Labeyrie, L., Vautravers, M., Duplessy, J.-C., Rossignol-Strick, M., Cortijo, E., Arnold,  
807 M. and Fontugne, M.: Hydrological relationship between the North Atlantic Ocean and the Mediterranean Sea  
808 during the past 15-75 kyr, *Paleoceanography*, 14(5), 626–638, doi:10.1029/1998PA900022, 1999.

809 Pérez-Folgado, M., Sierro, F. J., Flores, J. A., Cacho, I., Grimalt, J. O., Zahn, R. and Shackleton, N.: Western  
810 Mediterranean planktonic foraminifera events and millennial climatic variability during the last 70 kyr, *Mar.*  
811 *Micropaleontol.*, 48(1-2), 49–70, doi:10.1016/S0377-8398(02)00160-3, 2003.

812 Pinardi, N. and Masetti, E.: Variability of the large scale general circulation of the Mediterranean Sea from  
813 observations and modelling: a review, *Palaeogeogr. Palaeoclimatol. Palaeoecol.*, 158(3-4), 153–173,  
814 doi:10.1016/S0031-0182(00)00048-1, 2000.

815 Piotrowski, A. M., Galy, A., Nicholl, J. a. L., Roberts, N. L., Wilson, D. J., Clegg, J. a. and Yu, J.:  
816 Reconstructing deglacial North and South Atlantic deep water sourcing using foraminiferal Nd isotopes, *Earth*  
817 *Planet. Sci. Lett.*, 357-358, 289–297, doi:10.1016/j.epsl.2012.09.036, 2012.

818 Pons-Branchu, E., Douville, E., Roy-Barman, M., Dumont, E., Branchu, P., Thil, F., Frank, N., Bordier, L. and  
819 Borst, W.: A geochemical perspective on Parisian urban history based on U–Th dating, laminae counting and  
820 yttrium and REE concentrations of recent carbonates in underground aqueducts, *Quat. Geochronol.*, 24, 44–53,  
821 doi:10.1016/j.quageo.2014.08.001, 2014.

822 Prell, W. L.: Stability of low-latitude sea-surface temperatures: an evaluation of the CLIMAP reconstruction  
823 with emphasis on the positive SST anomalies. Final report, Providence, RI (USA)., 1985.

824 Reimer, P. J., Bard, E., Bayliss, A., Beck, J. W., Blackwell, P. G., Bronk Ramsey, C., Grootes, P. M.,  
825 Guilderson, T. P., Hafliðason, H., Hajdas, I., HattĹ, C., Heaton, T. J., Hoffmann, D. L., Hogg, A. G., Hughen, K.  
826 A., Kaiser, K. F., Kromer, B., Manning, S. W., Niu, M., Reimer, R. W., Richards, D. A., Scott, E. M., Southon,  
827 J. R., Staff, R. A., Turney, C. S. M., & van der Plicht, J. (2013). IntCal13 and Marine13 Radiocarbon Age  
828 Calibration Curves 0-50,000 Years cal BP. *Radiocarbon*, 55(4).

829 Revel, M., Colin, C., Bernasconi, S., Combourieu-Nebout, N., Ducassou, E., Grousset, F. E., Rolland, Y.,  
830 Migeon, S., Bosch, D., Brunet, P., Zhao, Y. and Mascle, J.: 21,000 Years of Ethiopian African monsoon  
831 variability recorded in sediments of the western Nile deep-sea fan, *Reg. Environ. Chang.*, 14(5), 1685–1696,  
832 doi:10.1007/s10113-014-0588-x, 2014.

833 Revel, M., Ducassou, E., Skonieczny, C., Colin, C., Bastian, L., Bosch, D., Migeon, S. and Mascle, J.: 20,000  
834 years of Nile River dynamics and environmental changes in the Nile catchment area as inferred from Nile upper

835 continental slope sediments, *Quat. Sci. Rev.*, 130, 200–221, doi:10.1016/j.quascirev.2015.10.030, 2015.

836 Roberts, N. L., Piotrowski, A. M., McManus, J. F. and Keigwin, L. D.: Synchronous deglacial overturning and  
837 water mass source changes., *Science*, 327(2010), 75–78, doi:10.1126/science.1178068, 2010.

838 Rodrigo-Gámiz, M., Martínez-Ruiz, F., Rampen, S. W., Schouten, S. and Sinninghe Damsté, J. S.: Sea surface  
839 temperature variations in the western Mediterranean Sea over the last 20 kyr: A dual-organic proxy (U K' 37 and  
840 LDI) approach, *Paleoceanography*, 29(2), 87–98, doi:10.1002/2013PA002466, 2014.

841 Rodrigo-Gámiz, M., Martínez-Ruiz, F., Chiaradia, M., Jiménez-Espejo, F. J. and Ariztegui, D.: Radiogenic  
842 isotopes for deciphering terrigenous input provenance in the western Mediterranean, *Chem. Geol.*, 410, 237–250,  
843 doi:10.1016/j.chemgeo.2015.06.004, 2015.

844 Rogerson, M., Rohling, E. J., Weaver, P. P. E. and Murray, J. W.: Glacial to interglacial changes in the settling  
845 depth of the Mediterranean Outflow plume, *Paleoceanography*, 20(3), doi:10.1029/2004PA001106, 2005.

846 Rogerson, M., Rohling, E. J. and Weaver, P. P. E.: Promotion of meridional overturning by Mediterranean-  
847 derived salt during the last deglaciation, *Paleoceanography*, 21(4), 1–8, doi:10.1029/2006PA001306, 2006.

848 Rogerson, M., Cacho, I., Jimenez-Espejo, F., Reguera, M. I., Sierro, F. J., Martinez-Ruiz, F., Frigola, J. and  
849 Canals, M.: A dynamic explanation for the origin of the western Mediterranean organic-rich layers,  
850 *Geochemistry, Geophys. Geosystems*, 9(7), n/a–n/a, doi:10.1029/2007GC001936, 2008.

851 Rohling, E. J.: Review and new aspects concerning the formation of eastern Mediterranean sapropels, *Mar.*  
852 *Geol.*, 122(1-2), 1–28, doi:10.1016/0025-3227(94)90202-X, 1994.

853 Rohling, E. J., Jorissen, F. J. and De stichter, H. C.: 200 Year interruption of Holocene sapropel formation in the  
854 Adriatic Sea, *J. Micropalaeontology*, 16(2), 97–108, doi:10.1144/jm.16.2.97, 1997.

855 Rohling, E. J., Mayewski, P. a, Abu-Zied, R. H., Casford, J. S. L. and Hayes, A.: Holocene atmosphere-ocean  
856 interactions: records from Greenland and the Aegean Sea, *Clim. Dyn.*, 18(7), 587–593, doi:10.1007/s00382-001-  
857 0194-8, 2002.

858 Rohling, E. J., Sprovieri, M., Cane, T., Casford, J. S. ., Cooke, S., Bouloubassi, I., Emeis, K. C., Schiebel, R.,  
859 Rogerson, M., Hayes, A., Jorissen, F. . and Kroon, D.: Reconstructing past planktic foraminiferal habitats using  
860 stable isotope data: a case history for Mediterranean sapropel S5, *Mar. Micropaleontol.*, 50(1-2), 89–123,  
861 doi:10.1016/S0377-8398(03)00068-9, 2004.

862 Rohling, E. J., Marino, G. and Grant, K. M.: Mediterranean climate and oceanography, and the periodic  
863 development of anoxic events (sapropels), *Earth-Science Rev.*, 143, 62–97, doi:10.1016/j.earscirev.2015.01.008,  
864 2015.

865 Rossignol-Strick, M., Nesteroff, W., Olive, P. and Vergnaud-Grazzini, C.: After the deluge: Mediterranean  
866 stagnation and sapropel formation, *Nature*, 295(5845), 105–110, doi:10.1038/295105a0, 1982.

867 Sammari, C., Millot, C., Taupier-Letage, I., Stefani, A. and Brahim, M.: Hydrological characteristics in the

- 868 Tunisia–Sardinia–Sicily area during spring 1995, *Deep Sea Res. Part I Oceanogr. Res. Pap.*, 46(10), 1671–1703,  
869 doi:10.1016/S0967-0637(99)00026-6, 1999.
- 870 Sarmiento, J. L., Herbert, T. and Toggweiler, J. R.: Mediterranean nutrient balance and episodes of anoxia,  
871 *Global Biogeochem. Cycles*, 2(4), 427–444, doi:10.1029/GB002i004p00427, 1988.
- 872
- 873 Sánchez-Goñi, M., Cacho, I., Turon, J. L., Guiot, J., Sierro, F. J., Peyrouquet, J., Grimalt, J. O. and Shackleton,  
874 N. J.: Synchronicity between marine and terrestrial responses to millennial scale climatic variability during the  
875 last glacial period in the Mediterranean region, *Clim. Dyn.*, 19(1), 95–105, doi:10.1007/s00382-001-0212-x,  
876 2002.
- 877 Sarnthein, M., Tetzlaff, G., Koopmann, B., Wolter, K. and Pflaumann, U.: Glacial and interglacial wind regimes  
878 over the eastern subtropical Atlantic and North-West Africa, *Nature*, 293, 193–196, doi:10.1038/293193a0,  
879 1981.
- 880 Scheuven, D., Schütz, L., Kandler, K., Ebert, M. and Weinbruch, S.: Bulk composition of northern African dust  
881 and its source sediments — A compilation, *Earth-Science Rev.*, 116, 170–194,  
882 doi:10.1016/j.earscirev.2012.08.005, 2013.
- 883 Schmiedl, G., Kuhnt, T., Ehrmann, W., Emeis, K. C., Hamann, Y., Kotthoff, U., Dulski, P. and Pross, J.:  
884 Climatic forcing of eastern Mediterranean deep-water formation and benthic ecosystems during the past 22 000  
885 years, *Quat. Sci. Rev.*, 29(23-24), 3006–3020, doi:10.1016/j.quascirev.2010.07.002, 2010.
- 886 Schönfeld, J. and Zahn, R.: Late Glacial to Holocene history of the Mediterranean outflow. Evidence from  
887 benthic foraminiferal assemblages and stable isotopes at the Portuguese margin, *Palaeogeogr. Palaeoclimatol.*  
888 *Palaeoecol.*, 159(1-2), 85–111, doi:10.1016/S0031-0182(00)00035-3, 2000.
- 889 Schott, F., Visbeck, M., Send, U., Fischer, J., Stramma, L. and Desaubies, Y.: Observations of Deep Convection  
890 in the Gulf of Lions, Northern Mediterranean, during the Winter of 1991/92, *J. Phys. Oceanogr.*, 26(4), 505–524,  
891 doi:10.1175/1520-0485(1996)026<0505:OODCIT>2.0.CO;2, 1996.
- 892 Schroeder, K., Millot, C., Bengara, L., Ben Ismail, S., Bensi, M., Borghini, M., Budillon, G., Cardin, V.,  
893 Coppola, L., Curtil, C., Drago, A., El Moumni, B., Font, J., Fuda, J. L., García-Lafuente, J., Gasparini, G. P.,  
894 Kontoyiannis, H., Lefevre, D., Puig, P., Raimbault, P., Rougier, G., Salat, J., Sammari, C., Sánchez Garrido, J.  
895 C., Sanchez-Roman, A., Sparnocchia, S., Tamburini, C., Taupier-Letage, I., Theocharis, A., Vargas-Yáñez, M.  
896 and Vetrano, A.: Long-term monitoring programme of the hydrological variability in the Mediterranean Sea: a  
897 first overview of the HYDROCHANGES network, *Ocean Sci.*, 9(2), 301–324, doi:10.5194/os-9-301-2013,  
898 2013.
- 899 Scrivner, A. E., Vance, D. and Rohling, E. J.: New neodymium isotope data quantify Nile involvement in  
900 Mediterranean anoxic episodes, *Geology*, 32(7), 565, doi:10.1130/G20419.1, 2004.
- 901 Shanahan, T. M., McKay, N. P., Hughen, K. A., Overpeck, J. T., Otto-Bliesner, B., Heil, C. W., King, J., Scholz,  
902 C. A. and Peck, J.: The time-transgressive termination of the African Humid Period, *Nat. Geosci.*, 8(2), 140–144,



903 doi:10.1038/ngeo2329, 2015.

904 Siani, G., Paterne, M., Arnold, M., Bard, E., Metivier, B., Tisnerat, N. and Bassinot, F.: Radiocarbon reservoir  
905 ages in the Mediterranean Sea and Black Sea, *Radiocarbon*, 42(2), 271–280 [online] Available from: <Go to  
906 ISI>://000089971000010, 2000.

907 Siani, G., Paterne, M., Michel, E., Sulpizio, R., Sbrana, A., Arnold, M. and Haddad, G.: Mediterranean Sea  
908 surface radiocarbon reservoir age changes since the last glacial maximum., *Science* (80-. ), 294(5548), 1917–  
909 1920, doi:10.1126/science.1063649, 2001.

910 Siani, G., Sulpizio, R., Paterne, M. and Sbrana, A.: Tephrostratigraphy study for the last 18,000 C years in a  
911 deep-sea sediment sequence for the South Adriatic, *Quat. Sci. Rev.*, 23(23-24), 2485–2500,  
912 doi:10.1016/j.quascirev.2004.06.004, 2004.

913 Siani, G., Magny, M., Paterne, M., Debret, M., Fontugne, M. (2013) - Paleohydrology reconstruction and  
914 Holocene climate variability in the South Adriatic Sea. *Climate of the Past*, 9, 499-515.

915 Sierro, F. J., Hodell, D. A., Curtis, J. H., Flores, J. A., Reguera, I., Colmenero-Hidalgo, E., Bárcena, M. A.,  
916 Grimalt, J. O., Cacho, I., Frigola, J. and Canals, M.: Impact of iceberg melting on Mediterranean thermohaline  
917 circulation during Heinrich events, *Paleoceanography*, 20(2), n/a–n/a, doi:10.1029/2004PA001051, 2005.

918 Sparnocchia, S., Gasparini, G. P., Astraldi, M., Borghini, M. and Pistek, P.: Dynamics and mixing of the Eastern  
919 Mediterranean outflow in the Tyrrhenian basin, *J. Mar. Syst.*, 20(1-4), 301–317, doi:10.1016/S0924-  
920 7963(98)00088-8, 1999.

921 Spivack, A. J. and Wasserburg, G. J.: Neodymium isotopic composition of the Mediterranean outflow and the  
922 eastern North Atlantic, *Geochim. Cosmochim. Acta*, 52(12), 2767–2773, doi:10.1016/0016-7037(88)90144-5,  
923 1988.

924 Stratford, K., Williams, R. G. and Myers, P. G.: Impact of the circulation on Sapropel Formation in the eastern  
925 Mediterranean, *Global Biogeochem. Cycles*, 14(2), 683–695, doi:10.1029/1999GB001157, 2000.

926 Stuiver, M., Reimer, P. J. and Reimer, R.: CALIB 7.0, *Radiocarb. Calibration Progr.*, 2005.

927 Tachikawa, K., Roy-Barman, M., Michard, A., Thouron, D., Yeghicheyan, D. and Jeandel, C.: Neodymium  
928 isotopes in the Mediterranean Sea: comparison between seawater and sediment signals, *Geochim. Cosmochim.*  
929 *Acta*, 68(14), 3095–3106, doi:10.1016/j.gca.2004.01.024, 2004.

930 Tachikawa, K., Piotrowski, A. M. and Bayon, G.: Neodymium associated with foraminiferal carbonate as a  
931 recorder of seawater isotopic signatures, *Quat. Sci. Rev.*, 88, 1–13, doi:10.1016/j.quascirev.2013.12.027, 2014.

932 Tanaka, T., Togashi, S., Kamioka, H., Amakawa, H., Kagami, H., Hamamoto, T., Yuhara, M., Orihashi, Y.,  
933 Yoneda, S., Shimizu, H., Kunimaru, T., Takahashi, K., Yanagi, T., Nakano, T., Fujimaki, H., Shinjo, R.,  
934 Asahara, Y., Tanimizu, M. and Dragusanu, C.: JNdi-1: a neodymium isotopic reference in consistency with  
935 LaJolla neodymium, *Chem. Geol.*, 168(3-4), 279–281, doi:10.1016/S0009-2541(00)00198-4, 2000.

- 936 Tachikawa, K., Vidal, L., Cornuault, M., Garcia, M., Pothin, A., Sonzogni, C., Bard, E., Menot, G. and Revel,  
937 M.: Eastern Mediterranean Sea circulation inferred from the conditions of S1 sapropel deposition, *Clim. Past*,  
938 11(6), 855–867, doi:10.5194/cp-11-855-2015, 2015.
- 939 Taviani, M., Angeletti, L., Canese, S., Cannas, R., Cardone, F., Cau, A., Cau, A. B., Follesa, M. C., Marchese,  
940 F., Montagna, P. and Tessarolo, C.: The “Sardinian cold-water coral province” in the context of the  
941 Mediterranean coral ecosystems, *Deep Sea Res. Part II Top. Stud. Oceanogr.*, doi:10.1016/j.dsr2.2015.12.008,  
942 2015.
- 943 Thunell, R. C. and Williams, D. F.: Glacial–Holocene salinity changes in the Mediterranean Sea: hydrographic  
944 and depositional effects, *Nature*, 338(6215), 493–496, doi:10.1038/338493a0, 1989.
- 945 Toucanne, S., Jouet, G., Ducassou, E., Bassetti, M. A., Dennielou, B., Angue Minto’o, C. M., Lahmi, M.,  
946 Touyet, N., Charlier, K., Lericolais, G. and Mulder, T.: A 130,000-year record of Levantine Intermediate Water  
947 flow variability in the Corsica Trough, western Mediterranean Sea, *Quat. Sci. Rev.*, 33, 55–73,  
948 doi:10.1016/j.quascirev.2011.11.020, 2012.
- 949 Vance, D., Scrivner, A. E. and Beney, P.: The use of foraminifera as a record of the past neodymium isotope  
950 composition of seawater, *Paleoceanography*, 19(2), PA2009, doi:10.1029/2003PA000957, 2004.
- 951 van de Flierdt, T., Robinson, L. F. and Adkins, J. F.: Deep-sea coral aragonite as a recorder for the neodymium  
952 isotopic composition of seawater, *Geochim. Cosmochim. Acta*, 74(21), 6014–6032,  
953 doi:10.1016/j.gca.2010.08.001, 2010.
- 954 Voelker, A. H. L., Lebreiro, S. M., Schönfeld, J., Cacho, I., Erlenkeuser, H. and Abrantes, F.: Mediterranean  
955 outflow strengthening during northern hemisphere coolings: A salt source for the glacial Atlantic?, *Earth Planet.*  
956 *Sci. Lett.*, 245, 39–55, doi:10.1016/j.epsl.2006.03.014, 2006.
- 957 Weaver, A. J., Saenko, O. a., Clark, P. U. and Mitrovica, J. X.: Meltwater Pulse 1A from Antarctica as a Trigger  
958 of the Bolling-Allerod Warm Interval, *Science* (80-. ), 299(5613), 1709–1713, doi:10.1126/science.1081002,  
959 2003.
- 960 Weldeab, S., Emeis, K.-C., Hemleben, C. and Siebel, W.: Provenance of lithogenic surface sediments and  
961 pathways of riverine suspended matter in the Eastern Mediterranean Sea: evidence from  $^{143}\text{Nd}/^{144}\text{Nd}$  and  
962  $^{87}\text{Sr}/^{86}\text{Sr}$  ratios, *Chem. Geol.*, 186(1-2), 139–149, doi:10.1016/S0009-2541(01)00415-6, 2002.
- 963 Weldeab, S., Menke, V. and Schmiedl, G.: The pace of East African monsoon evolution during the Holocene,  
964 *Geophys. Res. Lett.*, 41, 1724–1731, doi:10.1002/2014GL059361.Received, 2014.
- 965 Wienberg, C., Frank, N., Mertens, K. N., Stuut, J.-B. W., Marchant, M., Fietzke, J., Mienis, F. and Hebbeln, D.:  
966 Glacial cold-water coral growth in the Gulf of Cádiz: Implications of increased palaeo-productivity, *Earth*  
967 *Planet. Sci. Lett.*, 298(3-4), 405–416, doi:10.1016/j.epsl.2010.08.017, 2010.
- 968 Wu, Q., Colin, C., Liu, Z., Thil, F., Dubois-Dauphin, Q., Frank, N., Tachikawa, K., Bordier, L. and Douville, E.:  
969 Neodymium isotopic composition in foraminifera and authigenic phases of the South China Sea sediments:

970 Implications for the hydrology of the North Pacific Ocean over the past 25 kyr, *Geochemistry, Geophys.*  
971 *Geosystems*, 16(11), 3883–3904, doi:10.1002/2015GC005871, 2015.

## 972 **Table captions**

973

974 **Table 1.** U-series ages and  $\epsilon\text{Nd}$  values obtained for cold-water coral samples collected from sediment core RECORD 23  
975 (Sardinia Channel).

976

977 **Table 2.**  $\epsilon\text{Nd}$  values obtained for cold-water corals from the southern Alboran Sea. The AMS  $^{14}\text{C}$  ages published by Fink et  
978 al. (2013) are also reported as Median probability age (ka BP).

979

980 **Table 3.** AMS  $^{14}\text{C}$  ages of samples of the planktonic foraminifer *G. bulloides* from ‘off-mound’ sediment core SU92-33. The  
981 AMS  $^{14}\text{C}$  ages were corrected for  $^{13}\text{C}$  and a mean reservoir age of 400 yrs, and were converted into calendar years using the  
982 INTCAL13 calibration data set (Reimer et al., 2013) and the CALIB 7.0 program (Struiver et al., 2005).

983

984 **Table 4.** Multiproxy data obtained for the upper 2.1 m of sediment core SU92-33 (Balearic Sea). Stable oxygen and carbon  
985 isotopes were measured on benthic (*C. pachyderma*) and planktonic (*G. bulloides*) foraminifera;  $\epsilon\text{Nd}$  values were obtained on  
986 mixed planktonic foraminifera samples. The age results from a combination of 7 AMS- $^{14}\text{C}$  age measurements for the upper  
987 1.2 m of the core and by a linear interpolation between these ages as well as the  $\delta^{18}\text{O}$  variations of the planktonic  
988 foraminifera *G. bulloides*.

989

## 990 **Figure captions**

991

992 **Figure 1.** Map of the western Mediterranean Sea showing the locations of samples investigated in this study. Yellow dot  
993 indicates the sampling location of the sediment core from the Balearic Sea (SU92-33); yellow stars indicate the locations of  
994 the CWC-bearing cores from the Sardinia Channel (RECORD 23) and the southern Alboran Sea (for further details on the  
995 CWC from the Alboran Sea refer also to Fink et al., 2013). The cores discussed in this paper (Gulf of Cádiz: IODP site  
996 U1387, Balearic Sea: MD09-2343, northern Tyrrhenian Sea: MD01-2472, Adriatic Sea: MD90-917) are indicated by black  
997 dots, and seawater stations are marked by open squares. Arrows represent the main oceanographic currents. The black line  
998 shows the general trajectory of the Modified Atlantic Water (MAW) flowing at the surface from the Atlantic Ocean toward  
999 the western and eastern Mediterranean. The orange line represents the Levantine Intermediate Water (LIW) originating from  
1000 the eastern basin. The black dashed line shows the trajectory of the Western Mediterranean Deep Water (WMDW) flowing  
1001 from the Gulf of Lions toward the Strait of Gibraltar.

1002

1003 **Figure 2.** (a) Sea Surface Temperature (SST) records of cores SU92-33 (red line) and MD90-917 (green line; Siani et al.,  
1004 2004), (b)  $\delta^{18}\text{O}$  record obtained on planktonic foraminifer *G. bulloides* for core SU92-33, (c)  $\delta^{18}\text{O}$  record obtained on benthic  
1005 foraminifer *C. pachyderma* for core SU92-33, (d)  $\delta^{13}\text{C}$  record obtained on benthic foraminifer *C. pachyderma* for core SU92-  
1006 33. LGM: Last Glacial Maximum; HS1: Heinrich Stadial 1; B-A: Bølling-Allerød; YD: Younger Dryas. Black triangles  
1007 indicate AMS  $^{14}\text{C}$  age control points.

1008

1009 **Figure 3.** (a) Sea Surface Temperature (SST) record of core SU92-33 (red line), (b)  $\epsilon\text{Nd}$  records obtained on mixed  
1010 planktonic foraminifers from core SU92-33 (open circles) and from cold-water coral fragments collected in the Alboran Sea  
1011 (red squares), (c)  $\epsilon\text{Nd}$  values of cold-water corals from core RECORD 23 (Sardinia Channel).

1012

1013 **Figure 4.** (a)  $\delta^{13}\text{C}$  records obtained on benthic foraminifer *C. pachyderma* for cores SU92-33 (red line) and MD99-2343  
1014 (blue line; Sierro et al., 2005). (b)  $\epsilon\text{Nd}$  records obtained on mixed planktonic foraminifers from core SU92-33 (open circles)  
1015 and from cold-water coral fragments collected in the Alboran Sea (red squares). Modern  $\epsilon\text{Nd}$  values for LIW (orange dashed  
1016 line) and WMDW (blue dashed line) are also reported for comparison. (c)  $\epsilon\text{Nd}$  values obtained for planktonic foraminifera  
1017 with Fe-Mn coatings at sites 300G (36°21.532' N, 1°47.507' W; 1860 m; open dots) and 304G (36°19.873' N, 1°31.631' W;  
1018 2382 m; black dots) in Alboran Sea (Jimenez-Espejo et al., 2015). (d) UP10 fraction (>10  $\mu\text{m}$ ) from core MD99-2343  
1019 (Frigola et al., 2008). (e) Sortable silt mean grain-size of core MD01-2472 (Toucanne et al., 2012). (f) Ln Zr/Al ratio at IODP  
1020 site U1387 (36°48.3' N 7°43.1' W; 559 m) (Bahr et al., 2015).

1021  
1022 **Figure 5.** (a)  $\delta^{18}\text{O}$  record obtained on planktonic foraminifer *G. bulloides* for core SU92-33, (b)  $\delta^{13}\text{C}$  records obtained on  
1023 benthic foraminifer *C. pachyderma* for core SU92-33, (c)  $\epsilon\text{Nd}$  values of cold-water corals from core RECORD 23 (Sardinia  
1024 Channel), (d)  $\epsilon\text{Nd}$  values records obtained on mixed planktonic foraminifera from core SU92-33 (open circles) and from  
1025 cold-water coral fragments collected in the Alboran Sea (red squares), (e)  $\epsilon\text{Nd}$  values obtained on terrigenous fraction of  
1026 MS27PT located close the Nile River mouth in the eastern Mediterranean basin (Revel et al., 2015).  
1027

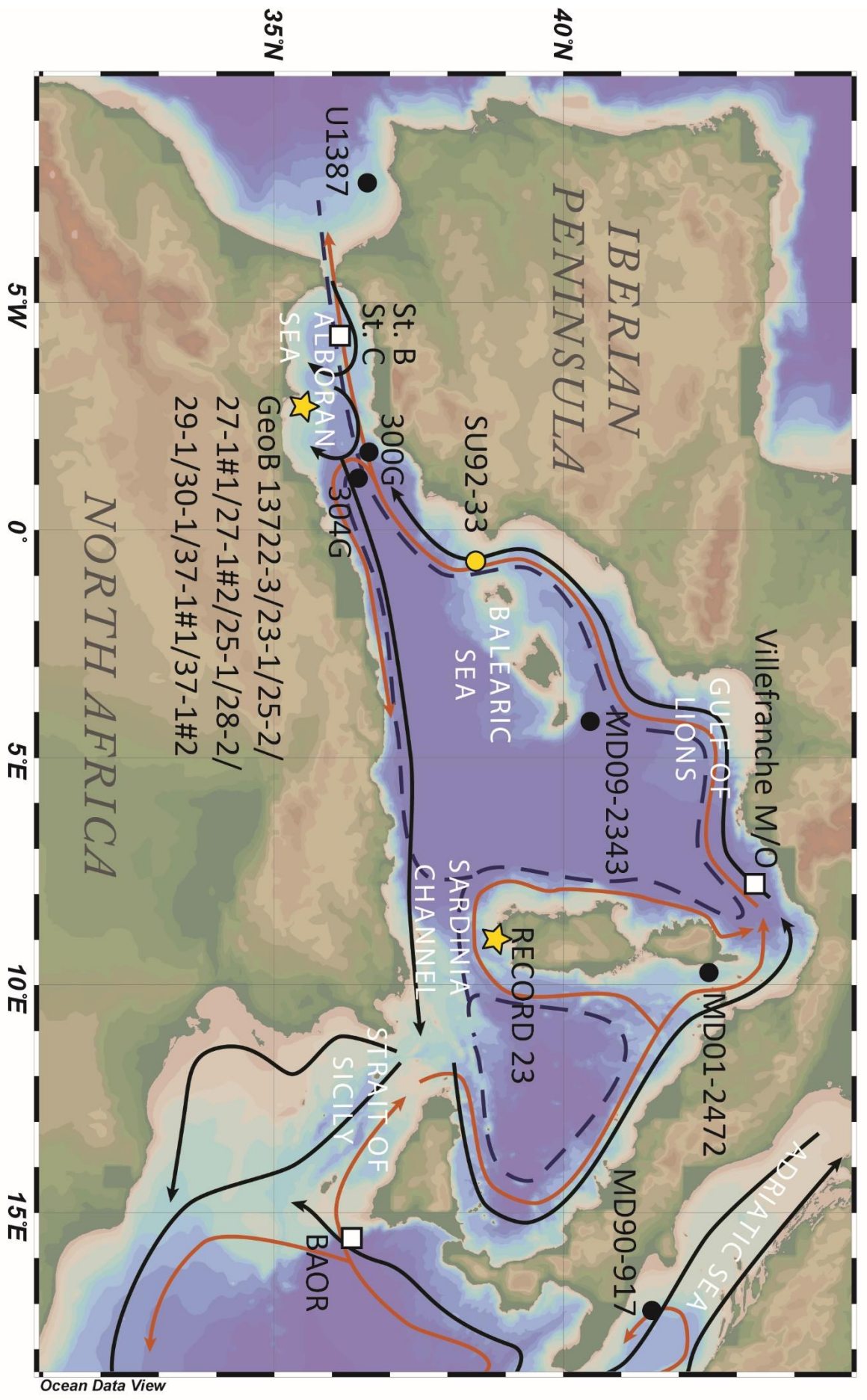


Figure 1

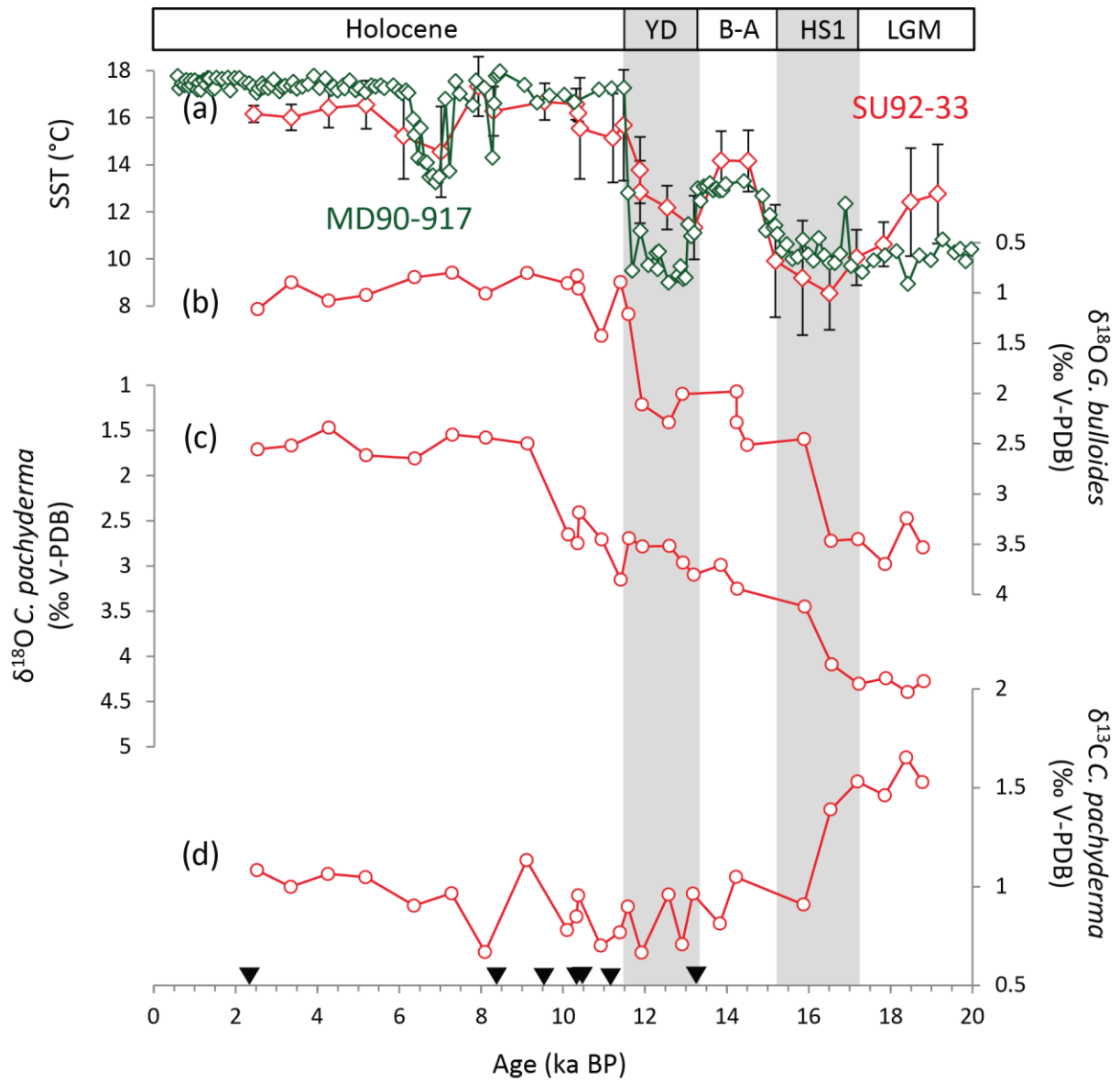


Figure 2

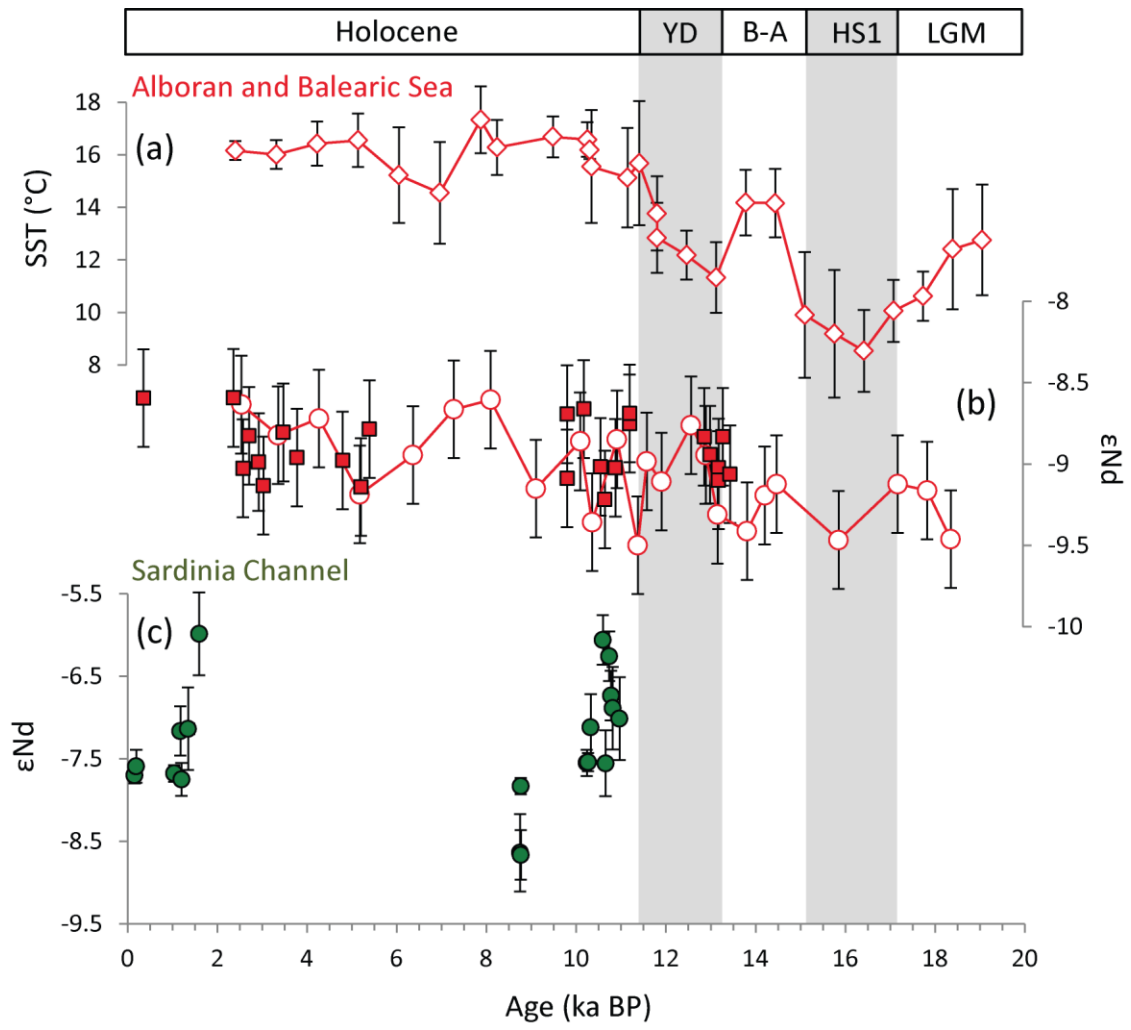


Figure 3

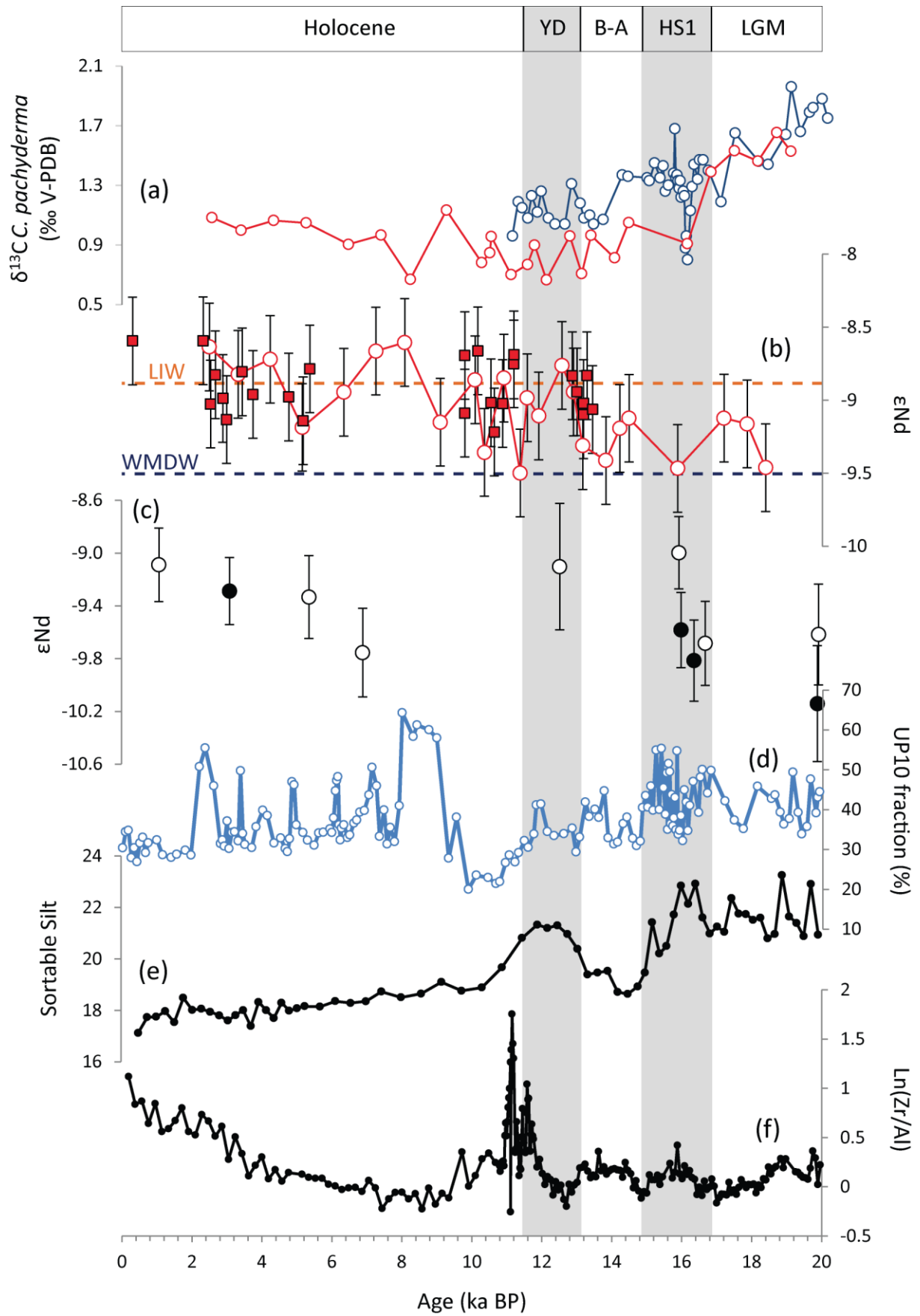


Figure 4



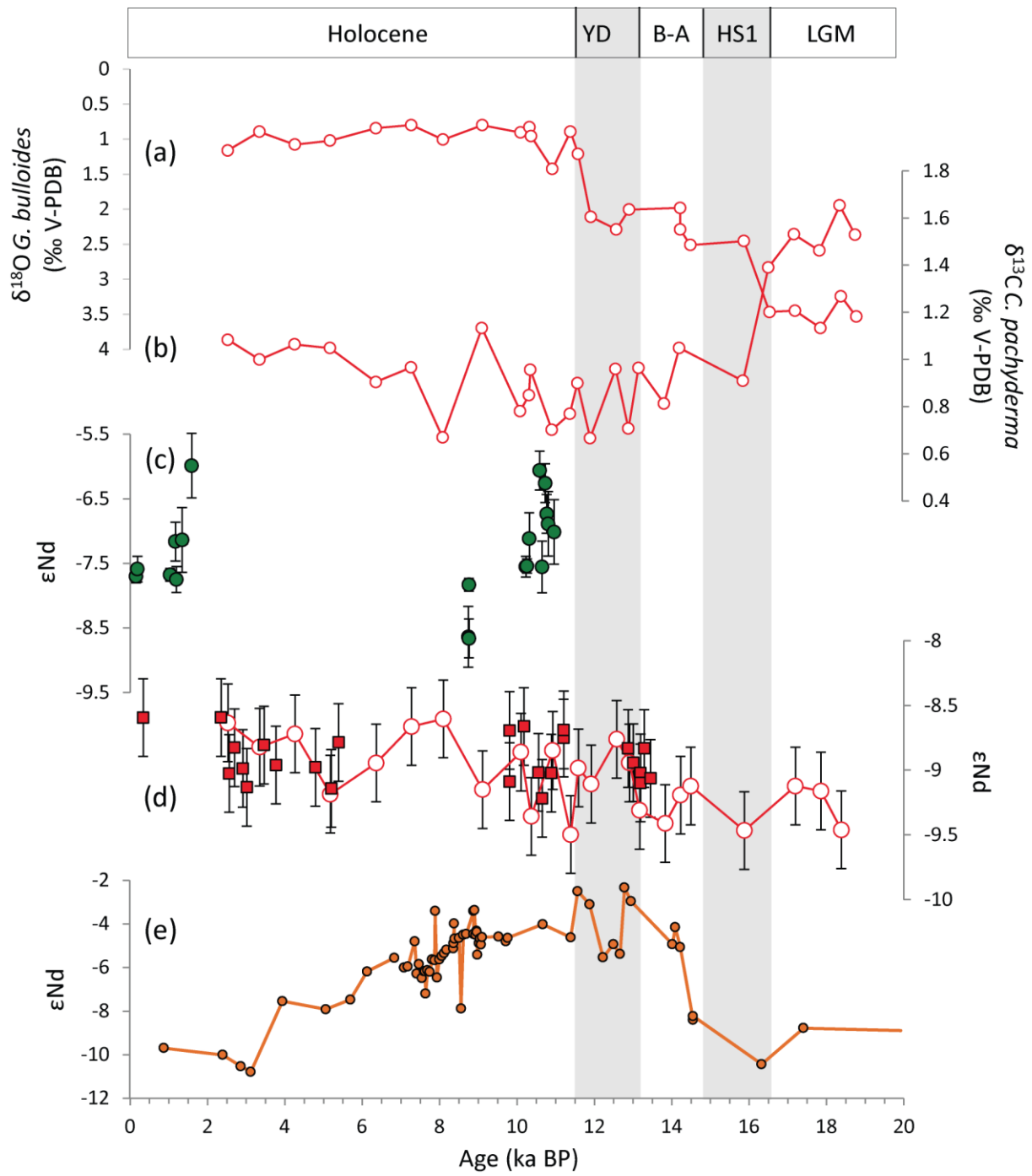


Figure 5

| Sample ID     | Depth in core (cm) | Corals species           | $^{238}\text{U}$ ( $\mu\text{g/g}$ ) | $^{232}\text{Th}$ ( $\text{ng/g}$ ) | $\delta^{234}\text{U}_m$ (‰) | $^{230}\text{Th}/^{238}\text{U}$ | $^{230}\text{Th}/^{232}\text{Th}$ | Age (ka BP)        | $\delta^{234}\text{U}_{(t)}$ (‰) | $^{143}\text{Nd}/^{144}\text{Nd}$ | $\epsilon\text{Nd}$ |
|---------------|--------------------|--------------------------|--------------------------------------|-------------------------------------|------------------------------|----------------------------------|-----------------------------------|--------------------|----------------------------------|-----------------------------------|---------------------|
| RECORD_23_V   | 0-3,5              | <i>Madrepora oculata</i> | 3.31 $\pm$ 0.005                     | 0.68 $\pm$ 0.014                    | 151.85 $\pm$ 1.7             | 0.00163 $\pm$ 0.00011            | 25 $\pm$ 1.7                      | 0.091 $\pm$ 0.011  | 151.92 $\pm$ 1.7                 | 0.512243 $\pm$ 0.000005           | -7.70 $\pm$ 0.10    |
| RECORD_23_V   | 3-7                | <i>Madrepora oculata</i> | 3.23 $\pm$ 0.002                     | 0.52 $\pm$ 0.001                    | 147.11 $\pm$ 0.6             | 0.00199 $\pm$ 0.00006            | 38 $\pm$ 1.1                      | 0.127 $\pm$ 0.006  | 147.19 $\pm$ 0.6                 | 0.512249 $\pm$ 0.000010           | -7.59 $\pm$ 0.20    |
| RECORD_23_V   | 7-10               | <i>Madrepora oculata</i> | 3.99 $\pm$ 0.007                     | 0.25 $\pm$ 0.002                    | 147.52 $\pm$ 1.7             | 0.01227 $\pm$ 0.00022            | 640 $\pm$ 11.6                    | 1.110 $\pm$ 0.023  | 148.01 $\pm$ 1.7                 | 0.512244 $\pm$ 0.000015           | -7.68 $\pm$ 0.30    |
| RECORD_23_V   | 8-10               | <i>Madrepora oculata</i> | 3.79 $\pm$ 0.005                     | 0.41 $\pm$ 0.001                    | 148.47 $\pm$ 0.7             | 0.01253 $\pm$ 0.00007            | 350 $\pm$ 2.0                     | 1.135 $\pm$ 0.008  | 148.27 $\pm$ 0.7                 | 0.512271 $\pm$ 0.000010           | -7.16 $\pm$ 0.20    |
| RECORD_23_IV  | 6-9                | <i>Madrepora oculata</i> | 4.06 $\pm$ 0.006                     | 0.35 $\pm$ 0.001                    | 148.47 $\pm$ 1.3             | 0.01366 $\pm$ 0.00011            | 480 $\pm$ 3.8                     | 1.243 $\pm$ 0.012  | 149.02 $\pm$ 1.2                 | 0.512241 $\pm$ 0.000010           | -7.75 $\pm$ 0.20    |
| RECORD_23_IV  | 27-30              | <i>Madrepora oculata</i> | 4.06 $\pm$ 0.003                     | 1.09 $\pm$ 0.001                    | 146.91 $\pm$ 1.1             | 0.01405 $\pm$ 0.00013            | 159 $\pm$ 1.4                     | 1.283 $\pm$ 0.014  | 147.47 $\pm$ 1.3                 | 0.512272 $\pm$ 0.000026           | -7.14 $\pm$ 0.50    |
| RECORD_23_IV  | 37-40              | <i>Madrepora oculata</i> | 3.52 $\pm$ 0.005                     | 0.08 $\pm$ 0.000                    | 148.25 $\pm$ 1.1             | 0.01663 $\pm$ 0.00012            | 2308 $\pm$ 16.4                   | 1.529 $\pm$ 0.013  | 148.92 $\pm$ 1.1                 | 0.512331 $\pm$ 0.000026           | -5.99 $\pm$ 0.50    |
| RECORD_23_III | 55-57              | <i>Madrepora oculata</i> | 3.63 $\pm$ 0.002                     | 0.27 $\pm$ 0.000                    | 145.30 $\pm$ 0.7             | 0.08859 $\pm$ 0.00020            | 3530 $\pm$ 8.1                    | 8.685 $\pm$ 0.027  | 148.93 $\pm$ 0.8                 | 0.512195 $\pm$ 0.000026           | -8.64 $\pm$ 0.50    |
| RECORD_23_III | 58-61              | <i>Madrepora oculata</i> | 4.24 $\pm$ 0.004                     | 0.36 $\pm$ 0.001                    | 146.71 $\pm$ 1.2             | 0.08863 $\pm$ 0.00037            | 3336 $\pm$ 14.0                   | 8.702 $\pm$ 0.048  | 150.39 $\pm$ 1.2                 | 0.512237 $\pm$ 0.000010           | -7.83 $\pm$ 0.20    |
| RECORD_23_III | 63-66              | <i>Lophelia pertusa</i>  | 4.15 $\pm$ 0.005                     | 0.42 $\pm$ 0.002                    | 147.19 $\pm$ 0.8             | 0.08863 $\pm$ 0.00054            | 2783 $\pm$ 17.1                   | 8.703 $\pm$ 0.063  | 150.89 $\pm$ 0.9                 | 0.512194 $\pm$ 0.000015           | -8.66 $\pm$ 0.30    |
| RECORD_23_I   | 0-2                | <i>Lophelia pertusa</i>  | 3.35 $\pm$ 0.002                     | 0.37 $\pm$ 0.000                    | 147.02 $\pm$ 0.7             | 0.10283 $\pm$ 0.00018            | 2788 $\pm$ 4.8                    | 10.173 $\pm$ 0.025 | 151.34 $\pm$ 0.7                 | 0.512251 $\pm$ 0.000010           | -7.55 $\pm$ 0.20    |
| RECORD_23_II  | 62-65              | <i>Lophelia pertusa</i>  | 3.27 $\pm$ 0.003                     | 0.39 $\pm$ 0.002                    | 144.75 $\pm$ 1.2             | 0.10289 $\pm$ 0.00061            | 2721 $\pm$ 16.1                   | 10.201 $\pm$ 0.075 | 149.01 $\pm$ 1.2                 | 0.512251 $\pm$ 0.000010           | -7.54 $\pm$ 0.20    |
| RECORD_23_II  | 50-52              | <i>Lophelia pertusa</i>  | 2.92 $\pm$ 0.003                     | 0.92 $\pm$ 0.003                    | 145.39 $\pm$ 1.6             | 0.10351 $\pm$ 0.00061            | 1046 $\pm$ 6.2                    | 10.260 $\pm$ 0.079 | 149.69 $\pm$ 1.6                 | 0.512273 $\pm$ 0.000021           | -7.12 $\pm$ 0.40    |
| RECORD_23_I   | 12-14              | <i>Lophelia pertusa</i>  | 3.07 $\pm$ 0.002                     | 0.49 $\pm$ 0.000                    | 145.22 $\pm$ 0.7             | 0.10609 $\pm$ 0.00023            | 1971 $\pm$ 4.3                    | 10.531 $\pm$ 0.031 | 149.64 $\pm$ 0.7                 | 0.512327 $\pm$ 0.000015           | -6.06 $\pm$ 0.30    |
| RECORD_23_I   | 5-7                | <i>Lophelia pertusa</i>  | 3.50 $\pm$ 0.002                     | 0.42 $\pm$ 0.000                    | 146.35 $\pm$ 0.9             | 0.10677 $\pm$ 0.00016            | 2654 $\pm$ 4.0                    | 10.591 $\pm$ 0.025 | 150.82 $\pm$ 0.9                 | 0.512251 $\pm$ 0.000021           | -7.55 $\pm$ 0.40    |
| RECORD_23_II  | 94-98              | <i>Lophelia pertusa</i>  | 3.14 $\pm$ 0.003                     | 0.62 $\pm$ 0.002                    | 146.42 $\pm$ 1.0             | 0.10755 $\pm$ 0.00047            | 1737 $\pm$ 7.6                    | 10.672 $\pm$ 0.059 | 150.94 $\pm$ 1.0                 | 0.512317 $\pm$ 0.000015           | -6.26 $\pm$ 0.30    |
| RECORD_23_I   | 15-17              | <i>Lophelia pertusa</i>  | 3.40 $\pm$ 0.003                     | 0.46 $\pm$ 0.000                    | 146.01 $\pm$ 0.9             | 0.10790 $\pm$ 0.00021            | 2409 $\pm$ 4.6                    | 10.713 $\pm$ 0.031 | 150.53 $\pm$ 0.9                 | 0.512293 $\pm$ 0.000015           | -6.73 $\pm$ 0.30    |
| RECORD_23_II  | 96-100             | <i>Lophelia pertusa</i>  | 3.61 $\pm$ 0.004                     | 0.35 $\pm$ 0.001                    | 145.50 $\pm$ 0.8             | 0.10821 $\pm$ 0.00044            | 3579 $\pm$ 14.7                   | 10.750 $\pm$ 0.055 | 150.02 $\pm$ 0.8                 | 0.512285 $\pm$ 0.000026           | -6.89 $\pm$ 0.50    |
| RECORD_23_II  | 93-95              | <i>Lophelia pertusa</i>  | 3.19 $\pm$ 0.003                     | 0.24 $\pm$ 0.000                    | 143.33 $\pm$ 0.8             | 0.10947 $\pm$ 0.00032            | 4381 $\pm$ 12.7                   | 10.904 $\pm$ 0.042 | 147.85 $\pm$ 0.9                 | 0.512279 $\pm$ 0.000026           | -7.01 $\pm$ 0.50    |

Table 1

| Sample ID      | Core depth (cm) | Species                  | Water Depth (m) | Median probability age (ka BP) | $^{143}\text{Nd}/^{144}\text{Nd}$ | $\epsilon\text{Nd}$ |
|----------------|-----------------|--------------------------|-----------------|--------------------------------|-----------------------------------|---------------------|
| GeoB 13727-1#1 | Surface         | <i>Lophelia pertusa</i>  | 363             | 0.339                          | 0.512198 ±0.000015                | -8.59 ±0.30         |
| GeoB 13727-1#2 | Surface         | <i>Madrepora oculata</i> | 353             | 2.351                          | 0.512198 ±0.000015                | -8.59 ±0.30         |
| GeoB 13730-1   | 6               | <i>Lophelia pertusa</i>  | 338             | 2.563                          | 0.512175 ±0.000015                | -9.03 ±0.30         |
| GeoB 13728-1   | Bulk (0-15)     | <i>Lophelia pertusa</i>  | 343             | 2.698                          | 0.512185 ±0.000015                | -8.83 ±0.30         |
| GeoB 13728-2   | 2               | <i>Lophelia pertusa</i>  | 343             | 2.913                          | 0.512177 ±0.000015                | -8.99 ±0.30         |
| GeoB 13722-3   | Bulk (0-15)     | <i>Madrepora oculata</i> | 280             | 3.018                          | 0.512170 ±0.000015                | -9.13 ±0.30         |
| GeoB 13722-3   | Bulk (15-30)    | <i>Madrepora oculata</i> | 280             | 3.463                          | 0.512186 ±0.000015                | -8.81 ±0.30         |
| GeoB 13735-1   | Bulk (0-15)     | <i>Madrepora oculata</i> | 280             | 3.770                          | 0.512179 ±0.000015                | -8.96 ±0.30         |
| GeoB 13723-1   | Bulk (0-8)      | <i>Madrepora oculata</i> | 291             | 4.790                          | 0.512178 ±0.000015                | -8.98 ±0.30         |
| GeoB 13725-2   | Surface         | <i>Madrepora oculata</i> | 355             | 5.201                          | 0.512169 ±0.000015                | -9.14 ±0.30         |
| GeoB 13723-1   | Bulk (8-20)     | <i>Madrepora oculata</i> | 291             | 5.390                          | 0.512187 ±0.000015                | -8.79 ±0.30         |
| GeoB 13729-1   | 2.5             | <i>Lophelia pertusa</i>  | 442             | 9.810                          | 0.512172 ±0.000015                | -9.09 ±0.30         |
| GeoB 13729-1   | 2.5             | <i>Lophelia pertusa</i>  | 442             | 9.810                          | 0.512193 ±0.000015                | -8.69 ±0.30         |
| GeoB 13729-1   | 49              | <i>Lophelia pertusa</i>  | 442             | 10.181                         | 0.512194 ±0.000015                | -8.66 ±0.30         |
| GeoB 13730-1   | 102             | <i>Lophelia pertusa</i>  | 338             | 10.556                         | 0.512176 ±0.000015                | -9.02 ±0.30         |
| GeoB 13730-1   | 194             | <i>Lophelia pertusa</i>  | 338             | 10.652                         | 0.512165 ±0.000015                | -9.22 ±0.30         |
| GeoB 13729-1   | 315             | <i>Lophelia pertusa</i>  | 442             | 10.889                         | 0.512176 ±0.000015                | -9.02 ±0.30         |
| GeoB 13729-1   | 375             | <i>Lophelia pertusa</i>  | 442             | 11.206                         | 0.512189 ±0.000015                | -8.75 ±0.30         |
| GeoB 13730-1   | 298             | <i>Lophelia pertusa</i>  | 338             | 11.208                         | 0.512193 ±0.000015                | -8.69 ±0.30         |
| GeoB 13728-2   | 191             | <i>Lophelia pertusa</i>  | 343             | 12.874                         | 0.512185 ±0.000015                | -8.83 ±0.30         |
| GeoB 13737-1#2 | Surface         | <i>Lophelia pertusa</i>  | 297             | 13.005                         | 0.512180 ±0.000015                | -8.94 ±0.30         |
| GeoB 13728-2   | 295             | <i>Lophelia pertusa</i>  | 364             | 13.194                         | 0.512176 ±0.000015                | -9.02 ±0.30         |
| GeoB 13728-2   | 295             | <i>Lophelia pertusa</i>  | 364             | 13.194                         | 0.512171 ±0.000015                | -9.10 ±0.30         |
| GeoB 13730-1   | 427             | <i>Lophelia pertusa</i>  | 338             | 13.291                         | 0.512185 ±0.000015                | -8.83 ±0.30         |
| GeoB 13737-1#1 | Surface         | <i>Lophelia pertusa</i>  | 299             | 13.452                         | 0.512174 ±0.000015                | -9.06 ±0.30         |

**Table 2**

| Core    | Depth in core (cm) | <sup>14</sup> C-age (years) | ±1σ (years) | Median probability age (ka BP) |
|---------|--------------------|-----------------------------|-------------|--------------------------------|
| SU92-33 | 0                  | 2770                        | 70          | 2437                           |
| SU92-33 | 64                 | 7870                        | 90          | 8280                           |
| SU92-33 | 70                 | 8670                        | 80          | 9528                           |
| SU92-33 | 74                 | 9510                        | 100         | 10295                          |
| SU92-33 | 84                 | 9610                        | 90          | 10389                          |
| SU92-33 | 90                 | 10180                       | 100         | 11192                          |
| SU92-33 | 120                | 11710                       | 110         | 13172                          |

**Table 3**

| Depth in core<br>(cm) | Age<br>(ka BP) | $\delta^{13}\text{C}$            |                                  | $\delta^{18}\text{O}$           |                                 | $^{143}\text{Nd}/^{144}\text{Nd}$ | $\epsilon\text{Nd}$ |
|-----------------------|----------------|----------------------------------|----------------------------------|---------------------------------|---------------------------------|-----------------------------------|---------------------|
|                       |                | <i>C. pachyderma</i><br>(‰ VPDB) | <i>C. pachyderma</i><br>(‰ VPDB) | <i>G. bulloides</i><br>(‰ VPDB) | <i>G. bulloides</i><br>(‰ VPDB) |                                   |                     |
| 1                     | 2.53           | 1.08                             | 1.71                             | -0.6                            | 1.16                            | 0.512195 ±0.000015                | -8.64 ±0.30         |
| 10                    | 3.35           | 1.00                             | 1.67                             | -0.82                           | 0.90                            | 0.512186 ±0.000015                | -8.82 ±0.30         |
| 19.5                  | 4.26           | 1.06                             | 1.47                             | -0.55                           | 1.08                            | 0.512191 ±0.000015                | -8.72 ±0.30         |
| 29.5                  | 5.18           | 1.05                             | 1.78                             | -0.55                           | 1.02                            | 0.512167 ±0.000015                | -9.19 ±0.30         |
| 42.5                  | 6.36           | 0.90                             | 1.81                             | -0.91                           | 0.84                            | 0.512179 ±0.000015                | -8.95 ±0.30         |
| 52.5                  | 7.28           | 0.97                             | 1.55                             | -0.80                           | 0.80                            | 0.512194 ±0.000015                | -8.66 ±0.30         |
| 61.5                  | 8.10           | 0.67                             | 1.58                             | -0.95                           | 1.01                            | 0.512197 ±0.000015                | -8.61 ±0.30         |
| 67.5                  | 9.11           | 1.13                             | 1.65                             | -1.07                           | 0.80                            | 0.512169 ±0.000015                | -9.15 ±0.30         |
| 72.5                  | 10.10          | 0.78                             | 2.65                             | -1.27                           | 0.91                            | 0.512184 ±0.000015                | -8.86 ±0.30         |
| 77.5                  | 10.33          | 0.85                             | 2.75                             | -1.10                           | 0.83                            | -                                 | -                   |
| 81.5                  | 10.37          | 0.96                             | 2.41                             | -1.21                           | 0.96                            | 0.512158 ±0.000015                | -9.36 ±0.30         |
| 87.5                  | 10.92          | 0.70                             | 2.71                             | -0.11                           | 1.43                            | 0.512184 ±0.000015                | -8.85 ±0.30         |
| 92.5                  | 11.39          | 0.77                             | 3.15                             | -1.00                           | 0.89                            | 0.512151 ±0.000015                | -9.50 ±0.30         |
| 95.5                  | 11.59          | 0.90                             | 2.69                             | -1.14                           | 1.21                            | 0.512178 ±0.000015                | -8.98 ±0.30         |
| 100.5                 | 11.92          | 0.67                             | 2.78                             | -0.44                           | 2.11                            | 0.512171 ±0.000015                | -9.11 ±0.30         |
| 110.5                 | 12.58          | 0.96                             | 2.78                             | -0.86                           | 2.29                            | 0.512189 ±0.000015                | -8.76 ±0.30         |
| 115.5                 | 12.91          | 0.71                             | 2.96                             | -0.54                           | 2.01                            | 0.512180 ±0.000015                | -8.94 ±0.30         |
| 119.5                 | 13.17          | 0.96                             | 3.09                             | -                               | -                               | 0.512161 ±0.000015                | -9.31 ±0.30         |
| 129.5                 | 13.83          | 0.81                             | 2.99                             | -                               | -                               | 0.512156 ±0.000015                | -9.41 ±0.30         |
| 135.5                 | 14.23          | 1.05                             | 3.25                             | -1.16                           | 1.98                            | 0.512167 ±0.000015                | -9.19 ±0.30         |
| 135.5                 | 14.23          | -                                | -                                | -0.94                           | 2.29                            | -                                 | -                   |
| 139.5                 | 14.49          | -                                | -                                | -0.96                           | 2.51                            | 0.512170 ±0.000015                | -9.12 ±0.30         |
| 159.5                 | 15.88          | 0.91                             | 3.45                             | -0.81                           | 2.45                            | 0.512153 ±0.000015                | -9.47 ±0.30         |
| 169.5                 | 16.54          | 1.39                             | 4.09                             | -0.76                           | 3.47                            | -                                 | -                   |
| 179.5                 | 17.20          | 1.53                             | 4.30                             | -0.98                           | 3.45                            | 0.512170 ±0.000015                | -9.12 ±0.30         |
| 190                   | 17.86          | 1.46                             | 4.24                             | -1.10                           | 3.70                            | 0.512168 ±0.000015                | -9.16 ±0.30         |
| 198                   | 18.39          | 1.65                             | 4.39                             | -1.24                           | 3.24                            | 0.512153 ±0.000015                | -9.46 ±0.30         |
| 206                   | 18.78          | 1.53                             | 4.28                             | -0.90                           | 3.53                            | -                                 | -                   |

**Table 4**